

Geochemistry, Geophysics, Geosystems®

RESEARCH ARTICLE

10.1029/2021GC009729

Key Points:

- $^{87}\text{Sr}/^{86}\text{Sr}$ of bulk sediment, Mn nodules, and fish teeth in the western North Pacific was analyzed to identify sedimentary end-members
- Bulk sediments consisted of dust, fish debris, and Mn oxides with volcanic components
- The introduction of volcanic components from the Izu-Bonin-Mariana arc increased in the latest Eocene

Supporting Information:

Supporting Information may be found in the online version of this article.

Correspondence to:

Y. Kato and K. Nakamura,
ykato@sys.t.u-tokyo.ac.jp;
kentaron@sys.t.u-tokyo.ac.jp

Citation:

Tanaka, E., Yasukawa, K., Nakamura, K., Ohta, J., Miyazaki, T., Vaglarov, B. S., et al. (2022). Secular variations in provenance of sedimentary components in the western North Pacific Ocean constrained by Sr isotopic features of deep-sea sediments. *Geochemistry, Geophysics, Geosystems*, 23, e2021GC009729. <https://doi.org/10.1029/2021GC009729>

Received 19 FEB 2021
 Accepted 23 NOV 2021

Author Contributions:

Conceptualization: Erika Tanaka, Kazutaka Yasukawa, Kentaro Nakamura, Junichiro Ohta, Takashi Miyazaki, Bogdan Stefanov Vaglarov, Hikaru Iwamori, Yasuhiro Kato
Data curation: Erika Tanaka, Kazutaka Yasukawa, Junichiro Ohta, Shiki Machida, Koichiro Fujinaga
Funding acquisition: Erika Tanaka, Kazutaka Yasukawa, Kentaro Nakamura, Yasuhiro Kato

© 2022. The Authors.

This is an open access article under the terms of the [Creative Commons Attribution License](https://creativecommons.org/licenses/by/4.0/), which permits use, distribution and reproduction in any medium, provided the original work is properly cited.

Secular Variations in Provenance of Sedimentary Components in the Western North Pacific Ocean Constrained by Sr Isotopic Features of Deep-Sea Sediments

Erika Tanaka^{1,2,3} , Kazutaka Yasukawa^{1,4} , Kentaro Nakamura^{1,3}, Junichiro Ohta^{3,4}, Takashi Miyazaki² , Bogdan Stefanov Vaglarov², Shiki Machida^{3,4} , Koichiro Fujinaga^{3,4}, Hikaru Iwamori^{5,6}, and Yasuhiro Kato^{1,3,4,7} 

¹Department of Systems Innovation, School of Engineering, The University of Tokyo, Bunkyo-ku, Japan, ²Research Institute for Marine Geodynamics, Japan Agency for Marine-Earth Science and Technology, Yokosuka, Japan, ³Ocean Resources Research Center for Next Generation, Chiba Institute of Technology, Narashino, Japan, ⁴Frontier Research Center for Energy and Resources, School of Engineering, The University of Tokyo, Bunkyo-ku, Japan, ⁵Earthquake Research Institute, The University of Tokyo, Bunkyo-ku, Japan, ⁶Department of Earth and Planetary Sciences, School of Science, Tokyo Institute of Technology, Meguro-ku, Japan, ⁷Submarine Resources Research Center, Research Institute for Marine Resources Utilization, Japan Agency for Marine-Earth Science and Technology, Yokosuka, Japan

Abstract Deep-sea sediments around Minamitorishima Island in the western North Pacific Ocean record the depositional environment in the central to western North Pacific since the late Cretaceous. Previous studies on the bulk chemical composition of deep-sea sediments in this area have revealed that the sediment column can be divided into five chemostratigraphic units with at least three intercalated layers enriched in rare-earth elements. However, the end-member components and their changes in abundance, which indicate compositional variation, as well as the environmental factors affecting them, remain unclear. Here, we report the bulk chemistry, including newly analyzed $^{87}\text{Sr}/^{86}\text{Sr}$ ratios of the sediments, seafloor Mn nodules, and fish teeth collected from the deep-sea basin around Minamitorishima Island, to identify the end-member components of the sediments. Our results suggest that the pelagic sediments in the study area are mainly composed of terrigenous components, hydrogenous Mn oxides, biogenic calcium phosphate, and volcanic materials. The combination of Sr isotope modeling and bulk chemistry revealed that the input of volcanic materials has increased twice, which might be Izu-Bonin-Mariana tephra of the latest Eocene to Oligocene explosive volcanism at the later event but is unclear at the earlier event. The provenance of terrigenous materials has changed from North America to East Asia. The bulk sediment chemostratigraphy around Minamitorishima Island could have resulted not only from the local environmental changes in the pelagic realm, but also from volcanism around the Pacific Ocean and the northwestward movement of the area due to the Pacific plate motion.

Plain Language Summary Deep-sea sediments around Minamitorishima (Marcus) Island in the western North Pacific Ocean record the depositional environment in the Pacific pelagic area for the past 75 million years. They comprise eight types of sediments with different chemical features, including three layers enriched in rare-earth elements. However, the origin of the different types of sediments in this region remains unclear. We measured the chemical compositions and Sr isotope ratios of the bulk sediments, Mn nodules, and fish teeth collected from the sediments to reveal the source materials of the sediments from the top layer to ~12 m below the seafloor. The results demonstrate that the source materials are composed of four components: dust from the continents, Mn oxides from seawater, fish teeth and bones, and volcanic components. Additionally, the sediment records indicate that long-term changes have occurred in the origins of volcanic materials and dust. We suggest that the input of volcanic materials, the changes in the dust source from America to Asia, and the Pacific plate motion may have significantly affected the deep-sea sediments in the study area.

1. Introduction

It is known that deep-sea sediments record various geochemical/mineralogical characteristics that could reflect environmental and geographic factors such as changes in water depth, distance from continents or tectonic plate boundaries (e.g., mid-ocean ridge and subduction zones), and paleoclimatic/paleoceanographic events (Dunlea,

Methodology: Erika Tanaka, Junichiro Ohta, Takashi Miyazaki, Bogdan Stefanov Vaglarov, Shiki Machida, Hikaru Iwamori

Project Administration: Kentaro Nakamura

Supervision: Kentaro Nakamura, Yasuhiro Kato

Visualization: Erika Tanaka, Koichiro Fujinaga

Writing – original draft: Erika Tanaka

Writing – review & editing: Erika Tanaka, Kazutaka Yasukawa, Kentaro Nakamura, Junichiro Ohta, Takashi Miyazaki, Bogdan Stefanov Vaglarov, Shiki Machida, Koichiro Fujinaga, Hikaru Iwamori, Yasuhiro Kato

Murray, Sauvage, Spivack, et al., 2015; Kato et al., 2011; Plank & Langmuir, 1998; Yasukawa et al., 2016; Zhou & Kyte, 1992). It is worth reconstructing the paleoceanographic/paleoenvironmental conditions of the western North Pacific because this area has moved from the central to the western Pacific since the late Cretaceous (Shipboard Scientific Party, 1990) and thus records the long-term evolution of the pelagic depositional environments in the Pacific Ocean.

In addition, rare earth elements and yttrium (REY)-enriched pelagic clay, which is called “REY-rich mud,” has been discovered and reported from the seafloor around Minamitorishima (Marcus) Island in the western North Pacific (Figure 1; Fujinaga et al., 2016; Iijima et al., 2016). It can be seen as a new REY resource owing to its high REY concentrations and immense resource potential (Takaya et al., 2018). To investigate the distribution of the REY-rich mud around Minamitorishima Island, over 70 piston core samples have been collected from this area in recent years (Fujinaga et al., 2016; Iijima et al., 2016; Takaya et al., 2018; Tanaka, Nakamura, Yasukawa, Mimura, Fujinaga, Iijima et al., 2020, Tanaka, Nakamura, Yasukawa, Mimura, Fujinaga, Ohta et al., 2020). Based on the bulk chemical compositions, Tanaka, Nakamura, Yasukawa, Mimura, Fujinaga, Iijima et al. (2020) concluded that deep-sea sediments around Minamitorishima Island can be systematically classified into five groups. In the studied cores, the sediment groups occurred in a certain sequence from the seafloor to depth, with three intercalated REY-enriched layers (REY peaks, defined as sediment with $\Sigma\text{REY} > 2,000$ ppm; Tanaka, Nakamura, Yasukawa, Mimura, Fujinaga, Iijima et al., 2020, Tanaka, Nakamura, Yasukawa, Mimura, Fujinaga, Ohta et al., 2020) that form a “multi-elemental chemostratigraphy” in the sediment column. The chemostratigraphic units and REY peaks classified by Tanaka, Nakamura, Yasukawa, Mimura, Fujinaga, Iijima et al. (2020) are described as follows, from the seafloor surface to depth: Units I and II, the 1st REY peak, Unit III, the 2nd REY peak, and Units IV and V intercalated by the 3rd REY peak. The characteristic chemical compositions of each unit and the REY peak could be attributed to variations in the proportions of the sediment source end-member components among the units (Tanaka, Nakamura, Yasukawa, Mimura, Fujinaga, Iijima et al., 2020). However, the chemical composition, provenance, and proportions of the sediment end-member components that exert control on the chemostratigraphy of the deep-sea sediments around Minamitorishima Island are not entirely clear because they hitherto have only been discussed with a focus on the bulk chemical and mineralogical compositions.

Radiogenic isotopes (e.g., Nd, Hf, Sr, and Pb isotopes) are well known as powerful tools to identify sediment source end-member components and their provenance. Each end-member component shows characteristic ratios of the isotopes that are independent of their chemical and mineralogical compositions (Godfrey, 2002; Miyazaki et al., 2016; van de Fliedert et al., 2004; Vervoort et al., 2011; Yasukawa et al., 2019). For example, the Sr isotopic ratios ($^{87}\text{Sr}/^{86}\text{Sr}$) are greater than 0.712 in the terrigenous component, whereas they are less than 0.705 in the volcanic components and ~ 0.7092 in modern seawater (Capo et al., 1998; Frank, 2002). Considering that deep-sea sediments are mixtures of such components, it may be suggested that the radiogenic isotopic ratios of the bulk sediment reflect the proportions of these single source components (i.e., end-member components), and thus the proportions can be determined quantitatively. Therefore, the mineralogical and chemical compositions and the radiogenic isotopic ratios of the sediments together can provide higher-resolution information on the origin, and thus the depositional history, of the sediments. Previous research applied radiogenic isotopes to the sediments in the western North Pacific, where the sediments similar to those in deep-sea basins around Minamitorishima exist, to discuss binary mixing between Chinese Loess and volcanic ash (Asahara, 1999; Asahara et al., 1999; Jones et al., 1994, 2000; Nakai et al., 1993). However, pelagic clay in the area around Minamitorishima Island also contains biogenic calcium phosphate (BCP) and hydrogenous Mn-oxides (Takaya et al., 2018; Yasukawa et al., 2020, 2021). Thus, for a comprehensive understanding of the depositional history of pelagic clay, various components should be discussed, which will place the pelagic clay research in a broader context than before. Furthermore, high-resolution datasets of the geochemical characteristics of pelagic clay, including the chemical compositions and isotope ratios, could provide detailed constraints not only on the Earth's surface geochemical cycles, but also on the subducting materials, and may thus describe the processes and nature involving them in the Earth's interior (Mimura et al., 2019; Plank et al., 2007; Plank & Langmuir, 1998).

Here, we present new Sr isotope analyses of bulk sediments, Mn nodules, and fish teeth collected from the deep-sea basin around Minamitorishima Island. Using geochemical data, including Sr isotope ratios and bulk chemical compositions, and microscopic observations, we estimated the contributions of the possible end-member

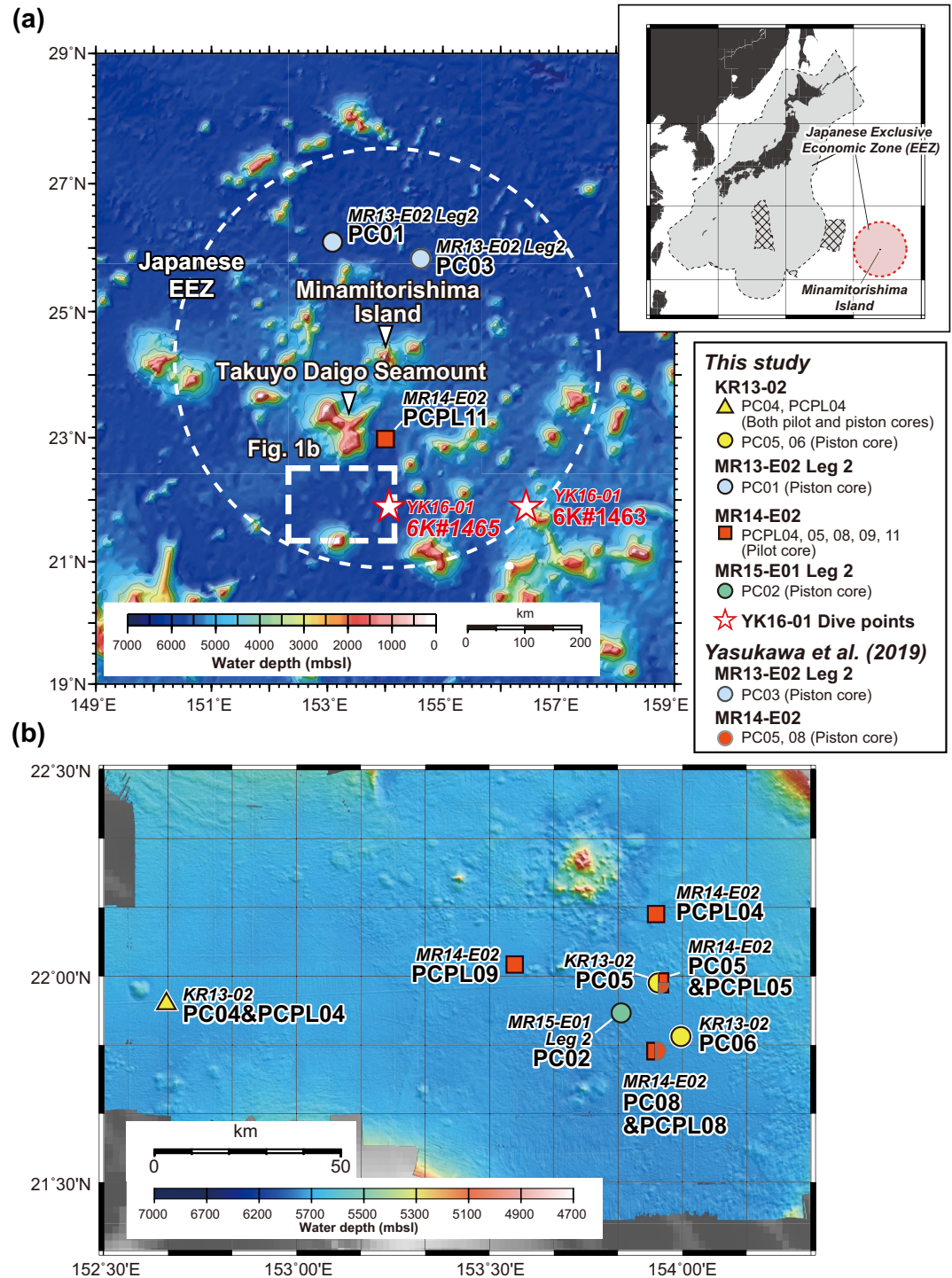


Figure 1. (a) Location of Minamitorishima Island and the regional bathymetry. White (in the left panel)- and red (in the right panel)-dashed circles represent the Japanese exclusive economic zone around Minamitorishima Island. The hatched area in the right panel indicates the extended continental shelf of Japan. (b) Enlarged view of the area in the white dashed rectangle shown in (a), along with bathymetry. Bathymetric data for (a) and (b) are from ETOPO1 (NOAA National Geophysical Data Center, 2009; <https://www.ngdc.noaa.gov/mgg/global/global.html>) and were obtained by multi-narrow-beam echo sounder (Machida, Sato, et al., 2021), respectively.

components and identified their origin and provenance using a quasi-quantitative method to analyze the transition and provenance of the sedimentary constituents and the environmental changes recorded in the deep-sea sediments in the western North Pacific Ocean.

2. Geological and Sedimentological Background

In the North Pacific pelagic realm, continental eolian dust is considered a major source of deep-sea sediments (Asahara et al., 1995; Kyte et al., 1993; Rea, 1994). Previous work demonstrated that the transport of eolian dust in the North Pacific has been affected by changes in atmospheric circulation patterns, such as the location of the Intertropical Convergence Zone (ITCZ; Pettke et al., 2000, 2002; Stancin et al., 2006; Hyeong et al., 2011, 2016; Zhang et al., 2016). Dust in the North Pacific has been supplied mainly by Asia, called Chinese Loess, in the past 25 million years following the aridification of the Asian interior (Zhang et al., 2016). Notably, Hyeong et al. (2016) reported that the dust source in the eastern North Pacific changed at the Eocene-Oligocene boundary; they attributed this shift to the potential migration of the ITCZ. In contrast, although the Asian continent has been considered the dust source of the sediments in the Minamitorishima area during the Quaternary and Pliocene periods (Asahara, 1999; Asahara et al., 1999), possible changes in the dust source throughout the Cenozoic remain poorly understood.

It is noteworthy that abnormal concentrations of BCP were observed in the deep-sea sediments around Minamitorishima Island (Iijima et al., 2016; Takaya et al., 2018). BCP is the main host of REY in deep-sea sediments and accounts for more than 20,000 ppm of Σ REY (Arrhenius et al., 1957; Bernat, 1975; Kashiwabara et al., 2014, 2018; Takaya et al., 2018; Toyoda et al., 1990). The high concentration of BCP results in the formation of REY peaks, including those in deep-sea sediments with Σ REY >5,000 ppm, which are called extremely REY-rich mud (Iijima et al., 2016; Takaya et al., 2018).

On the seafloor surface around Minamitorishima Island, precipitation of Fe–Mn (oxyhydr)oxide colloids from overlying seawater has formed Mn nodules and crusts, which are mainly of hydrogenetic origin (Azami et al., 2018; Machida, Sato, et al., 2021; Machia, Nakamura et al., 2021; Machida et al., 2016; A. Usui et al., 2017). These Fe–Mn (oxyhydr)oxides can adsorb and concentrate various metals on the mineral surface through ionic forces. Notably, highly oxidative Mn oxides (δ -MnO₂) of hydrogenetic origin support redox reactions and further concentrate several redox-sensitive elements (e.g., Co[II] to Co[III] and Ce[III] to Ce[IV]; Halbach & Puteanus, 1984; Hein & Koschinsky, 2014; Ohta & Kawabe, 2001; Takahashi et al., 2000, 2007). Also, oxic pelagic clay contains much smaller Fe–Mn (oxyhydr)oxide particles called Fe–Mn micronodules (several hundred micrometers in size) and Mn microparticles (several micrometers to submicrometer scale). Uramoto et al. (2019) reported abundant hydrogenetic Mn microparticles in oxic pelagic clays of the South Pacific Gyre. Yasukawa et al. (2020) estimated that oxic diagenetic Fe–Mn micronodules and hydrogenetic Mn microparticles accounted for 8%–50% and 50%–92%, respectively, of the Fe–Mn (oxyhydr)oxide content of the REY-rich mud south of Minamitorishima Island.

In addition, the deep-sea basins in the western North Pacific are surrounded by a number of seamounts and knolls, which could supply volcanic materials. Most of the seamounts in the western North Pacific were formed as hotspots in the area called the South Pacific Isotopic and Thermal Anomaly (5°S to 40°S, 105°W to 180°W) from 140 to 70 million years ago (Ma; Christie et al., 1995; Koppers et al., 2003). Today, the area with many Cretaceous seamounts in the western North Pacific is known as the West Pacific Seamount Province (WPSP; Koppers et al., 2003) and ranges from approximately 0°N to 35°N and 140°E to 175°E. In contrast, very young small knolls in the western North Pacific are called petit-spot volcanos (Hirano, 2011; Hirano et al., 2008, 2019). Those near Minamitorishima Island have an age of <3 Ma (Hirano et al., 2019). Moreover, the Izu-Bonin-Mariana (IBM) volcanic arc in the western North Pacific was activated by the subduction of the Pacific plate beneath the Philippine Sea plate from 52 to 48 Ma (Arculus et al., 2015; Ishizuka, Tani, et al., 2011; Taylor & Goodliffe, 2004). In the early stage, the IBM arc was aligned east-west near the equator; however, it gradually rotated to a north-south alignment and migrated northward (Hall, 2002; Taylor & Goodliffe, 2004). Recent studies revealed that the volcanism in the early stage was characterized by forearc basalt at 52.5 Ma, and boninite for the infant arc edifice building at 51.3–46 Ma (Arculus et al., 2015; Brandl et al., 2017; Brounce et al., 2021; Ishizuka, Tani, et al., 2011, 2018; Robertson et al., 2018), followed by the mature arc edifice building (40–28 Ma; Brandl et al., 2017; Johnson et al., 2021). In particular, the volcanism in the latest Eocene to early Oligocene (~37–28 Ma) was dominated by subaerial and subaqueous explosive volcanism producing the vitric

ash, accompanied by the growth of the initial Izu-Bonin-Mariana arc, including the section called the Kyushu-Palau Ridge (KPR; Shipboard Scientific Party, 2002; Johnson et al., 2021). The KPR volcanism decreased between ~25 and 22 Ma and stopped at ~22 Ma, at the same time as the formation of Shikoku and Parece Vela backarc basins (Ishizuka, Taylor, et al., 2011; Taylor, 1992). Notably, volcanic activity continued in the Mariana arc even after the temporary cessation of volcanism in the Izu-Bonin arc (Straub et al., 2015). After vigorous activity resumed in the Izu-Bonin arc ~17 Ma (Bryant et al., 2003), the IBM arc has been active, and explosive volcanism has continued (Ishizuka, Taylor, et al., 2011; Kutterolf et al., 2018; Robertson et al., 2018; Schindlbeck et al., 2018; Straub et al., 2010, 2015).

3. Materials and Methods

3.1. Cruise and Sample Information

In this study, bulk sediment samples obtained from five piston cores (KR13-02 PC04, PC05, and PC06; MR13-E02 Leg 2 PC01; and MR15-E01 Leg 2 PC02) and six pilot cores (KR13-02 PCPL04 and MR14-E02 PCPL04, PCPL05, PCPL08, PCPL09, and PCPL11) were analyzed, and all samples were collected within the Japanese exclusive economic zone (EEZ) around Minamitorishima Island during cruises KR13-02 of R/V Kairei and MR13-E02 Leg 2, MR14-E02, and MR15-E01 Leg 2 of R/V Mirai (Fujinaga et al., 2016; Iijima et al., 2016; Takaya et al., 2018; Tanaka, Nakamura, Yasukawa, Mimura, Fujinaga, Iijima et al., 2020). The sampling locations are shown in Figure 1 and are listed in Table S1 in Supporting Information S1. A piston corer consists of a 15-m long duralumin outerpipe and polycarbonate innertube, whereas a pilot corer is 2-m long exhibiting the same feature, and reaches the seafloor preceding the piston corer. For each site, the sediment lithology and physical properties of the pilot core and the topmost section of the piston core were generally identical. However, the sediment samples collected by pilot cores are more likely to retain detailed information around the topmost part of the sediment column, which is typically disturbed during piston coring.

We analyzed the $^{87}\text{Sr}/^{86}\text{Sr}$ of 38 bulk sediment samples from the five piston and six pilot cores noted above (Figure 2, Table S2 in Supporting Information S2). In addition, fish tooth samples were collected from 22 horizons in KR13-02 PC05, and their Sr isotopic ratios were analyzed. The sampling points of all bulk sediments and fish teeth are shown in Figure 2, with the lithologies and REY contents of the cores reported in previous studies (Fujinaga et al., 2016; Iijima et al., 2016; Takaya et al., 2018; Tanaka, Nakamura, Yasukawa, Mimura, Fujinaga, Iijima et al., 2020).

This study newly analyzed bulk chemical compositions of 13 samples from three piston cores (KR13-02 PC05, PC06, and MR15-E01 PC02) and six pilot cores (KR13-02 PCPL04 and MR14-E02 PCPL04, PCPL05, PCPL08, PCPL09, and PCPL11; Figure 2, Table S2 in Supporting Information S2) to obtain a higher sampling resolution than that described in previous studies to complement the bulk sediment data set in the target horizons for Sr isotopic analysis, and to obtain the geochemical information of the uppermost sediment layer in the studied area. The bulk chemical compositions of the other 25 samples were reported by Fujinaga et al. (2016), Iijima et al. (2016), Takaya et al. (2018), and Tanaka, Nakamura, Yasukawa, Mimura, Fujinaga, Iijima et al. (2020), and are listed in Table S2 in Supporting Information S2.

All of the cores in this study were collected below the carbonate compensation depth in the Pacific (~4.5 km; Van Andel, 1975; Pälke et al., 2012). The sediment samples are dark brown to blackish-dark brown and are categorized as pelagic clay or silty clay. Fujinaga et al. (2016), Iijima et al. (2016), Ohta et al. (2016, 2020), and Tanaka, Nakamura, Yasukawa, Mimura, Fujinaga, Iijima et al. (2020), Tanaka, Nakamura, Yasukawa, Mimura, Fujinaga, Ohta et al. (2020) reported the details of the lithology based on the microscopic observations (Figure 2). The main component of all cores is a clay-sized fraction of <4 μm . It is notable that the total proportions of silt-sized and sand-sized grains, which are mainly phillipsite and BCP, increase to >10% in the layers from 2.43 to 8.44 and 12.11–12.73 m below the seafloor (mbsf) in KR13-02 PC04, 0.50–3.67, and 6.82–11.45 mbsf in KR13-02 PC05, 0.50–3.00 mbsf, and 6.00–11.68 mbsf in KR13-02 PC06 (Fujinaga et al., 2016; Iijima et al., 2016; Ohta et al., 2016), and 0.00–1.96 mbsf in MR15-E01 Leg 2 PC02, respectively. The observed minor components are Fe–Mn micronodules, quartz, feldspar, reddish-brown semi-opaque oxides, colored unidentifiable minerals, radiolaria, diatoms, and siliceous sponge spicules. This study utilized the proportion of phillipsite based on the microscopic observations during/after the research cruises in Section 5.3.2, in addition to the reported data by Ohta et al. (2016, 2020). All protocols followed those described by the International Ocean Discovery Program (IODP)

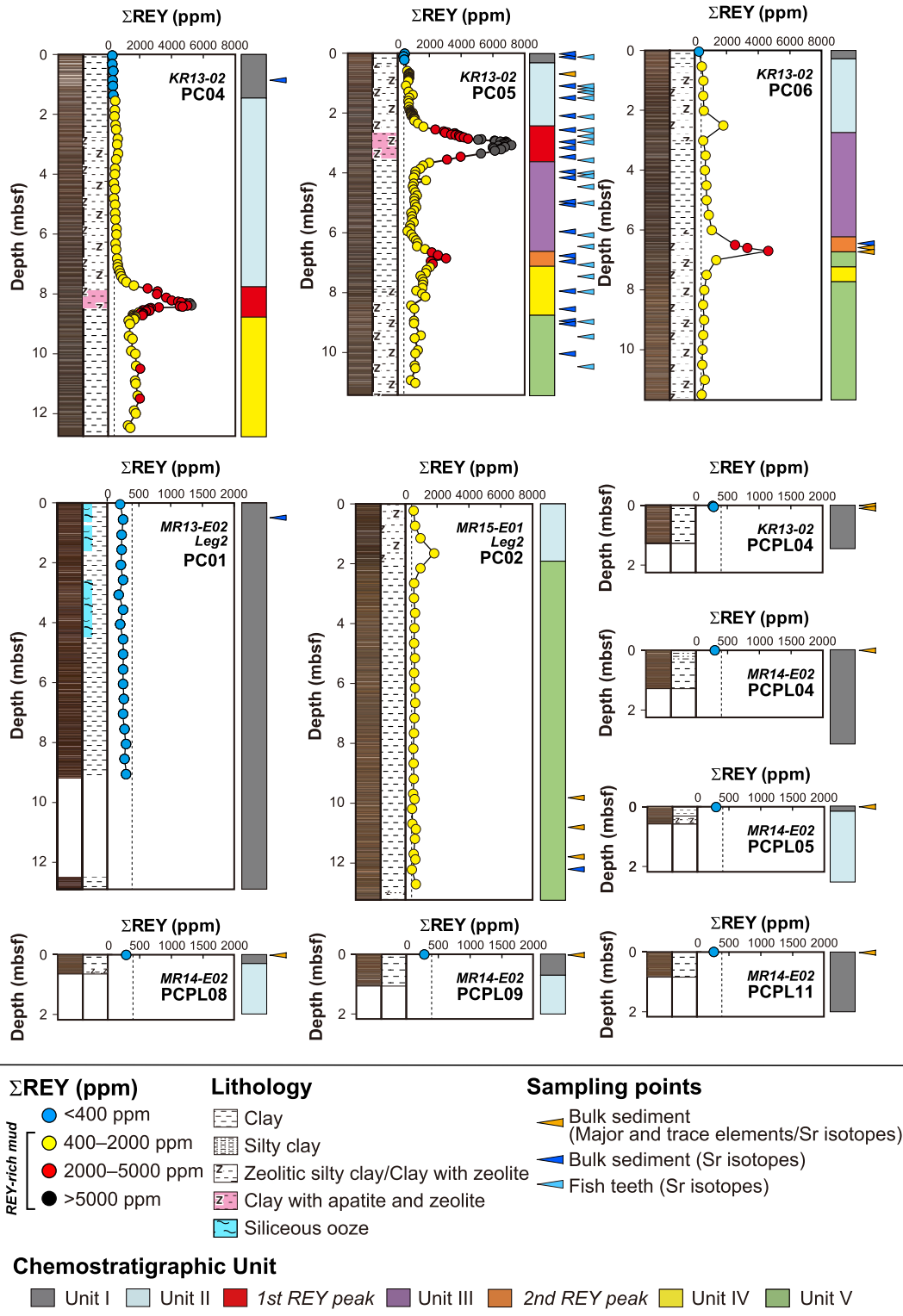


Figure 2. Lithology and total rare earth elements and yttrium (REY) contents of the studied cores reported by Fujinaga et al. (2016), Iijima et al. (2016), Takaya et al. (2018), Tanaka, Nakamura, Yasukawa, Mimura, Fujinaga, Iijima et al. (2020), and this study. Orange, blue, and light blue triangles indicate the sampling points for bulk sediments (major and trace elements, and Sr isotopes), bulk sediments (Sr isotopes), and fish teeth (Sr isotopes), respectively. The chemostratigraphic units next to the REY content of the piston cores are from Tanaka, Nakamura, Yasukawa, Mimura, Fujinaga, Iijima et al. (2020). In addition, the chemostratigraphic units next to the REY content of the pilot cores are those of top 2 m of KR13-02 PC04 and MR14-E02 PC04, PC05, PC08, PC09, and PC11 from Tanaka, Nakamura, Yasukawa, Mimura, Fujinaga, Iijima et al. (2020), respectively.

by Mazzullo and Graham (1988) in the same manner as Ohta et al. (2016), and we estimated the proportions of all constituents visually and normalized the values to 100% in total.

Tanaka, Nakamura, Yasukawa, Mimura, Fujinaga, Iijima et al. (2020) reported chemostratigraphic classification of the sediments in the study area using the following definitions (Fe_2O_3^* represents total iron content expressed as Fe_2O_3):

- Unit I: Ba (ppm) > Co (ppm) + 330 (ppm), and ΣREY (ppm) < 400
- Unit II: TiO_2 (wt.%) > 0.7, and ΣREY (ppm) > 400
- 1st REY peak: ΣREY (ppm) > 2,000 between Unit II and III
- Unit III: Fe_2O_3^* (wt.%) / TiO_2 (wt.%) > 11, and ΣREY (ppm) > 400
- 2nd REY peak: ΣREY (ppm) > 2,000 between Unit III and IV
- Unit IV: P_2O_5 (wt.%) / ΣREY (ppm) > 0.0018, and ΣREY (ppm) > 400
- Unit V: the remaining samples
- 3rd REY peak: ΣREY (ppm) > 2,000 in Unit IV or V

The units and REY peaks form the sequence in a descending order, as mentioned above, except for the intercalation of Units IV and V, and the 3rd REY peak. The chemostratigraphy of the samples in this study is shown in Figure 2 and Table S2 in Supporting Information S2. Based on the chemostratigraphic correlation among the cores, most of the cores lack one or more of the units, as defined above (Tanaka, Nakamura, Yasukawa, Mimura, Fujinaga, Iijima et al., 2020; Tanaka, Nakamura, Yasukawa, Mimura, Fujinaga, Ohta et al., 2020). We attribute these omissions to local erosion. In the study cores, KR13-02 PC04 lacks Units III, V, and 2nd/3rd REY peaks, PC05 lacks the 3rd REY peak, and PC06 lacks the 1st/3rd REY peaks. Moreover, MR13-E02 Leg2 PC01 contains only Unit I, and MR15-E01 Leg2 PC02 contains only Unit II and V. Although the pilot cores have not been classified in the previous studies, the simple comparison between piston cores and pilot cores suggests that KR13-02 PCPL04, MR14-E02 PCPL04, and PCPL11 could only contain Unit I, whereas MR14-E02 PCPL05, PCPL08, and PCPL09 could contain Units I and II (Figure 2). Based on the chemostratigraphic observations, this study selected samples from multiple cores to cover the variation of the chemostratigraphic units and REY peaks, in addition to intensive sampling from KR13-02 PC05.

The depositional ages of Units I and II, and the 1st REY peak are constrained by the Os isotope and ichthyolith stratigraphies of the two piston cores in this area (KR13-02 PC05 and MR14-E02 PC11; Nozaki et al., 2019; Ohta et al., 2020). Based on them, it is suggested that the bottom of Unit I corresponds to ~11 Ma at KR13-02 PC05 and 12.0 Ma at MR14-E02 PC11; Unit II was deposited between 20.0 and 34.08 Ma at KR13-02 PC05 and between 15.0 and 34.0 Ma at MR14-E02 PC11; the 1st REY peak was deposited between 34.16 and 34.6 Ma at KR13-02 PC05 and between ~34.0 and ~35.0 Ma at MR14-E02 at MR14-E02 PC11. Although there are uncertainties owing to possible erosion(s) (Tanaka, Nakamura, Yasukawa, Mimura, Fujinaga, Iijima et al., 2020; Tanaka, Nakamura, Yasukawa, Mimura, Fujinaga, Ohta et al., 2020), it is suggested that Unit I was deposited after 12 Ma, Unit II was deposited between at least ~15 and ~34 Ma, and the 1st REY peak was deposited just before the Eocene–Oligocene boundary. On the other hand, Usui and Yamazaki (2021) reported paleomagnetic constraints for the initiation of the 1st REY peak deposition, from 38.615 Ma to 34.999 Ma during the latest Eocene, indicating that further investigations would be required to determine the precise age and sedimentation rate of the REY peak.

Moreover, we analyzed the $^{87}\text{Sr}/^{86}\text{Sr}$ ratios of two Mn nodules, 6K#1463 N2-007 and 6K#1465 N4-003, which were collected by the submersible SHINKAI 6500 during dives 6K#1463 and 6K#1465, respectively, within the Minamitorishima EEZ (Machida, Sato, et al., 2021, Figure 1). The dives were conducted during Cruise YK16-01 of R/V Yokosuka from April 8 to 27, 2016. During dive 6K#1463, a spherical Mn nodule, 6K#1463 N2-007, was collected from the foot of a small seamount (5,457 m below sea level; mbsl) at the southeastern end of the Minamitorishima EEZ (Figure 1, Table S3 in Supporting Information S1). During dive 6K#1465, an oval Mn nodule, 6K#1465 N4-003, was collected from a small mound at 5,679 mbsl near the location of KR13-02 PC05 (Figure 1, Table S3 in Supporting Information S1). The texture of both nodules consists of three layers, L0, L1, and L2, which were identified by Machida et al. (2016). In this study, we determined the $^{87}\text{Sr}/^{86}\text{Sr}$ values of five subsamples from 6K#1463 N2-007 (one subsample from L0, two from L1, and two from L2) and three from 6K#1465 N4-003 (one subsample each from L0, L1, and L2; Figure S1 in Supporting Information S1).

3.2. Methods

The bulk sediment samples were dried at 110°C prior to the analysis. In contrast to fish tooth samples (see below), they were not acid-leached before digestion. They were prepared by the glass bead method using $\text{Li}_2\text{B}_4\text{O}_7$ as a flux and LiBr as a releasing agent for major-element analyses (Kato et al., 1998, 2002; Yasukawa et al., 2014), by mix-acid ($\text{HF-HNO}_3\text{-HClO}_4$ and $\text{HNO}_3\text{-HCl-HF}$) digestions for trace-element analyses (Kato et al., 2005; Yasukawa et al., 2014, 2019), and by acid digestion and purification using HF, HNO_3 , HClO_4 , and HCl for Sr isotope analyses (Miyazaki et al., 2018). Mn nodule samples were leached using 2.5 M HCl following the methods for Mn crusts described by Ling et al. (2005) and Amakawa et al. (2017) to extract elements associated with hydrogenous Mn oxides. Hand-picked fish tooth samples were precleaned by (a) reductive, (b) oxidative, and (c) acetic acid cleaning to remove (a) oxyhydroxides, (b) organic matters and opal, and (c) carbonate on the sample surface, following Gleason et al. (2002), and completely digested using HNO_3 . The leachate and digested samples of Mn oxides and fish teeth were prepared using the same method as that for the bulk sediment samples.

Major- and trace-element analyses were conducted at the Department of Systems Innovation, the University of Tokyo. The major-element content was determined using X-ray fluorescence (XRF) spectrometry (Rigaku ZSX Primus II) following the methods described by Kato et al. (1998, 2002) and Yasukawa et al. (2014). The trace-element content was determined using inductively coupled plasma quadrupole mass spectrometry (ICP-QMS; Thermo Fisher Scientific i-CAP Q) following Kato et al. (2005) and Yasukawa et al. (2014, 2019). The analytical results were within 3% for major elements and generally within 5% for trace elements (relative percent difference) of the accepted values reported for the Geological Survey of Japan (GSJ) reference materials JB-1b and JB-2, respectively.

Digestion and purification for Sr isotopic analysis were conducted in a Level 100 clean room at Japan Agency for Marine-Earth Science and Technology (JAMSTEC) mainly following Miyazaki et al. (2018). Sr separation was performed using the AG50W-X8 cation ion-exchange resin (Bio-Rad, California, USA) and the Sr-spec resin (Eichrom Technologies, Inc., Illinois, USA). Column separation was performed using a fully automated open-column chemical separation system called COLUMNSPIDER, which was developed by JAMSTEC and HOYUTEC Co., Ltd. (Kawagoe, Japan; Miyazaki et al., 2012). Sr isotopes were measured via thermal ionization mass spectrometry using the TRITON TI[®] instrument (Thermo-Finnigan, Bremen, Germany) at JAMSTEC following Takahashi et al. (2009). The mean $^{87}\text{Sr}/^{86}\text{Sr}$ values of the standard reference materials from the US National Institute of Standards and Technology SRM 987, and GSJ JB-2, and JMn-1 were 0.710241 ± 0.000024 (2 S.E., $n = 34$), 0.703674 ± 0.000025 (2 S.E., $n = 12$), and 0.709178 ± 0.000020 (2 S.E., $n = 1$), respectively. The total procedural blank concentration was below 35.9 pg. The analytical details are presented in Text S1 in Supporting Information S1.

4. Results

4.1. Chemical Compositions of Bulk Sediments

The major- and trace-element contents of 13 bulk sediment samples analyzed in this study are in the range of previously reported data for the study area (Table S2 in Supporting Information S2; Fujinaga et al., 2016; Iijima et al., 2016; Takaya et al., 2018; Tanaka, Nakamura, Yasukawa, Mimura, Fujinaga, Iijima et al., 2020). On the basis of the chemostratigraphic unit classification proposed by Tanaka, Nakamura, Yasukawa, Mimura, Fujinaga, Iijima et al. (2020), a sample from KR13-02 PC05, two samples from KR13-02 PC06, and three samples from MR15-E01 PC02, whose major- and trace-element contents were measured in this study (Figure 2), could be categorized as Unit II, the 2nd REY peak, and Unit V, respectively (Table S2 in Supporting Information S2). In contrast, all seven samples from the top of the pilot cores (Figure 2) are identified as the topmost unit, that is, Unit I (Table S2 in Supporting Information S2). The post-Archean average Australian shale-normalized (PAAS; Pourmand et al., 2012) REY patterns of the six samples from KR13-02 PC05, PC06, and MR15-E01 PC02 (i.e., Unit II, the 2nd REY peak, and Unit V, respectively; Figure S2 in Supporting Information S1) show negative Ce anomalies with relative enrichment of heavy rare earth elements; however, three Unit V samples from MR15-E01 PC02 have smaller negative Ce anomalies than those reported in the previous studies (Figure S2 in Supporting Information S1). In addition, the seven samples from the pilot cores (i.e., Unit I) do not show a clear Ce anomaly (Figure S2 in Supporting Information S1).

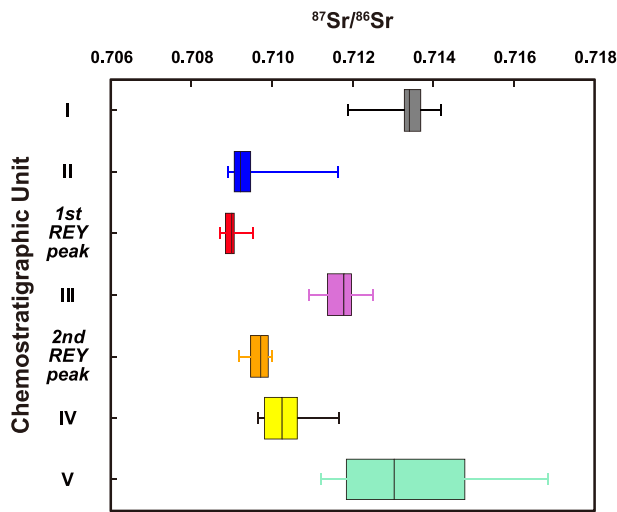


Figure 3. Box plot of bulk Sr isotopic values of each chemostratigraphic unit in the studied area. The analyzed data are from this study and from Yasukawa et al. (2019), and the chemostratigraphic classification is based on the method reported by Tanaka, Nakamura, Yasukawa, Mimura, Fujinaga, Iijima et al. (2020). The left and right edges of each box represent the 25th and 75th percentiles, respectively. The line in the middle of each box represents the average value. In addition, the left and right edges of the bar indicate minimum and maximum values, respectively.

4.2. Sr Isotopic Ratios of Bulk Sediments, Mn Nodules, and Fish Teeth

The Sr isotopic ratios of the 38 bulk sediment samples are listed in Table S2 in Supporting Information S2. The maximum value was 0.716845 at 12.22 mbsf in MR15-E01 PC02, whereas the minimum was 0.708715 at 3.17 mbsf in KR13-02 PC05. In terms of the chemostratigraphy (Figure 3, Table S2 in Supporting Information S2), the samples from Units I and V showed higher Sr values ($^{87}\text{Sr}/^{86}\text{Sr} > 0.712$) than the samples from Unit II and the REY peaks ($^{87}\text{Sr}/^{86}\text{Sr} < 0.710$). The samples from Units III and IV presented with intermediate values ranging between 0.710 and 0.712. Notably, $^{87}\text{Sr}/^{86}\text{Sr}$ ratios of the four Unit V samples from MR15-E01 are highest among all the samples ($^{87}\text{Sr}/^{86}\text{Sr} = 0.714424\text{--}0.716845$), which is higher than those of the other Unit V samples by 0.002–0.004.

Figures 4a and 4b illustrate the downhole variation of $^{87}\text{Sr}/^{86}\text{Sr}$ of bulk sediments in KR13-02 PC04 and PC05. They include 13 Sr-isotope data reported by Yasukawa et al. (2019), along with 23 new data obtained in this study. In KR13-02 PC04, the bulk $^{87}\text{Sr}/^{86}\text{Sr}$ decreases from 0.713370 at 0.85 mbsf to approximately 0.7090 at 7.00–8.37 mbsf. However, $^{87}\text{Sr}/^{86}\text{Sr}$ is slightly higher below the 1st REY peak than at 7.00–8.37 mbsf ($^{87}\text{Sr}/^{86}\text{Sr} = 0.710710$ at 10.37 mbsf and 0.710310 at 10.97 mbsf; Figure 4a). In KR13-02 PC05, the sample near the surface shows the highest value ($^{87}\text{Sr}/^{86}\text{Sr} = 0.714183$ at 0.13 mbsf), whereas the samples collected from Unit II and the 1st REY peak at 0.70–3.47 mbsf have values of less than 0.7100 (Figure 4b). The values for the sediments of Unit III are intermediate ($^{87}\text{Sr}/^{86}\text{Sr} = 0.710907\text{--}0.712485$ at 3.97–6.07 mbsf; Figure 4b). The samples collected from the 2nd REY peak

and the middle of Unit IV show low values ($^{87}\text{Sr}/^{86}\text{Sr} = 0.709642\text{--}0.709650$ at 6.77–7.96 mbsf), whereas those collected from the bottom of Units IV and V show higher values ($^{87}\text{Sr}/^{86}\text{Sr} = 0.711637\text{--}0.713033$ at 8.56–11.05 mbsf).

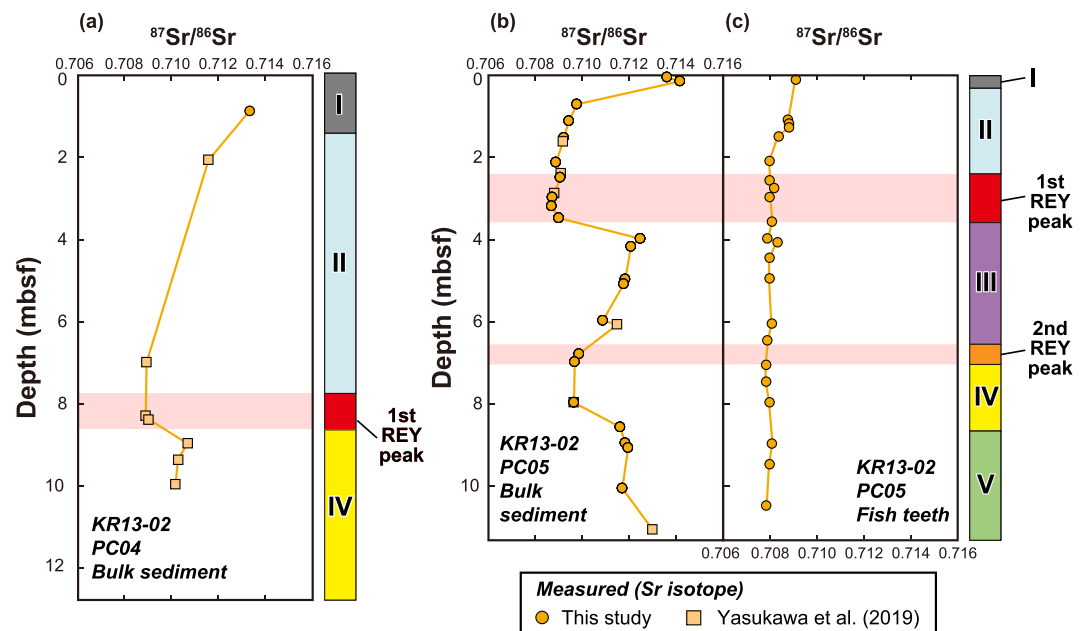


Figure 4. Downhole variation of Sr isotopic ratios of (a) bulk sediment samples in KR13-02 PC04, (b) bulk sediment samples in KR13-02 PC05, and (c) fish tooth samples in KR13-02 PC05. As for (a) and (b), 23 samples shown as circles are from this study, and 13 samples represented as squares are from Yasukawa et al. (2019).

The leachates from eight Mn nodules have almost homogenous $^{87}\text{Sr}/^{86}\text{Sr}$ values of 0.709096–0.709181 (Table S4a in Supporting Information S2). In contrast, most of the fish tooth samples exhibit lower $^{87}\text{Sr}/^{86}\text{Sr}$ values than those obtained for the Mn nodule leachates (0.707854–0.709123; Table S4b in Supporting Information S2). In the depth profile of KR13-02 PC05 (Figure 4c), the $^{87}\text{Sr}/^{86}\text{Sr}$ values of the fish teeth decrease from 0.709123 at 0.13 mbsf to 0.708402 at 1.50 mbsf, although they are less variable below 2.12 mbsf (less than approximately 0.7084).

5. Discussion

5.1. Geochemical Characteristics of the Fish Teeth and Mn Nodule Samples

First, we discuss the geochemical characteristics, in particular the Sr isotopic ratios, of the fish teeth and Mn nodule samples around Minamitorishima Island. The range of Sr isotopic ratios of the fish teeth in this study ($^{87}\text{Sr}/^{86}\text{Sr} = 0.707854\text{--}0.709123$) are similar to those in the seawater $^{87}\text{Sr}/^{86}\text{Sr}$ records during the Cenozoic reported by Veizer et al. (1999), Frank (2002), and McArthur et al. (2012, 2020). Strontium isotope ratios in pelagic seawater were homogenous at each age, regardless of the location, because the residence time of Sr ($>10^6$ years) is sufficiently longer than the timescale of ocean circulations (several hundred to 1,500 years; Broecker & Peng, 1982; Frank, 2002; Ravizza & Zachos, 2014). However, considering the depositional ages of Units I and II, and the 1st REY peak (Middle Miocene to Pliocene, Oligocene to Early Miocene, and the latest Eocene to the Eocene–Oligocene boundary, respectively; Nozaki et al., 2019; Ohta et al., 2020; Usui & Yamazaki, 2021), the $^{87}\text{Sr}/^{86}\text{Sr}$ values of the fish teeth could be higher (0.709123 in Unit I, 0.708015–0.708837 in Unit II, and 0.708022–0.708189 in the 1st REY peak) than those in seawater at each plausible time interval of deposition (0.708250–0.709050 during the Middle Miocene to Pliocene, 0.707850 to 0.708250 during the Oligocene to Early Miocene, and 0.707800 to 0.707900 during the latest Eocene to the Eocene–Oligocene boundary; Veizer et al., 1999; McArthur et al., 2012, 2020). Therefore, it is likely that the fish teeth did not perfectly preserve the marine Sr isotopic values at the time of deposition. A possible reason for the shift to higher Sr isotopic ratios is the effects of diagenetic alteration by pore water (Ingram, 1995; Martin & Scher, 2004). Although the degree of alteration of fish teeth in pelagic clay by pore water in this area has not been assessed, we have accepted the measured values as the limits of the range of Sr isotopic ratios maintained by fish teeth in the sediments in this study.

In contrast, all of the Mn nodule leachate samples show very similar Sr isotopic ratios ($^{87}\text{Sr}/^{86}\text{Sr} = 0.709096\text{--}0.709181$; Table S4 in Supporting Information S2), as noted in Section 4.2. These values are close to those of modern seawater (Frank, 2002; McArthur et al., 2012; Veizer et al., 1999) and a Mn nodule on the sediment surface reported in previous research (Ito et al., 1998). This similarity could be attributed to the continuous exchange of Sr between the leachable Mn oxide phase and the surrounding seawater, regardless of the origin of the Mn oxide (i.e., whether it is hydrogenous, diagenetic, or hydrothermal; Clauer et al., 1984; Ito et al., 1998). Therefore, the Mn nodules in this study could also reflect Sr isotopes in modern seawater.

5.2. Geochemical Characteristics of Bulk Sediment Samples

5.2.1. Continental Components

The geochemical characteristics of the bulk sediment samples are described on the basis of $^{87}\text{Sr}/^{86}\text{Sr}$ ratios and the PAAS-normalized REY patterns. The bulk sediment samples show significant variations in $^{87}\text{Sr}/^{86}\text{Sr}$, which ranges from 0.708715 (at 3.17 mbsf in KR13-02 PC05) to 0.716845 (at 12.22 mbsf in MR15-E01 PC02; Figure 3, Table S2 in Supporting Information S2). This variation can be attributed to variable mixtures of the end-members. The $^{87}\text{Sr}/^{86}\text{Sr}$ of samples from the uppermost and lowermost sediment layers (Units I and V; Tanaka, Nakamura, Yasukawa, Mimura, Fujinaga, Iijima et al., 2020) are relatively high (>0.712 ; Figure 3, Table S2 in Supporting Information S2). In contrast, the sediments in Units II to IV have lower $^{87}\text{Sr}/^{86}\text{Sr}$ values than those in Units I and V (Figure 3, Table S2 in Supporting Information S2), suggesting an increase in the proportion of components with low $^{87}\text{Sr}/^{86}\text{Sr}$ ratios or a decrease in the proportion of components with high $^{87}\text{Sr}/^{86}\text{Sr}$ ratios in Units II to IV.

Possible components with high Sr isotopic ratios are continental rocks, which generally have high $^{87}\text{Sr}/^{86}\text{Sr}$ values ($^{87}\text{Sr}/^{86}\text{Sr} > 0.712$; Chen et al., 2007; Gallet et al., 1996; Jahn et al., 2001; Kanayama et al., 2005; McCulloch & Wasserburg, 1978; Pearce et al., 2015; Sun, 2005; Yokoo et al., 2004); the values in Units I and V are consistent with this range. The PAAS-normalized REY patterns of the Unit I samples are almost flat (Figure S2 in Supporting Information S1). In addition, previous studies have reported the predominance of terrigenous material in Unit

I, specifically from the Chinese Loess Plateau or Taklimakan desert (Tanaka, Nakamura, Yasukawa, Mimura, Fujinaga, Iijima et al., 2020; Yasukawa et al., 2019). Therefore, the high $^{87}\text{Sr}/^{86}\text{Sr}$ values of the bulk sediments in Unit I are mainly attributed to terrigenous material from East Asia. In contrast, the bulk REY concentrations in Unit V are higher than those in Unit I (Figure S2, Table S2 in Supporting Information S2) and are generally in the same range as those in Units II to IV. This result suggests that the $^{87}\text{Sr}/^{86}\text{Sr}$ values of Unit V could result from the mixing of terrigenous materials with higher $^{87}\text{Sr}/^{86}\text{Sr}$ values than those in Unit I and other materials with relatively low $^{87}\text{Sr}/^{86}\text{Sr}$ values.

5.2.2. Proportions of BCP and Mn Oxides in Bulk Sediment

In this section, we discuss the mixing proportions of the terrigenous components and other possible constituents on the basis of the characteristic element compositions. Here, we assume that the eolian dust of Chinese Loess (Table S5 in Supporting Information S2; Chen et al., 2007; Gallet et al., 1996; Jahn et al., 2001; Sun & Zhu, 2010; Taylor et al., 1983; Yokoo et al., 2004) is a modern, plausible terrigenous end-member of the pelagic sediments in the study area. This is because the Unit I samples are dominated by the terrigenous component, as suggested in Section 5.2.1, which seems to reflect the final deposition of materials as a result of wind-driven dust transport from Asia (Asahara, 1999; Asahara et al., 1999; Yasukawa et al., 2019; Zhang et al., 2016).

For other possible end-member constituents, we next focus on BCP as the main host of REY in the deep-sea sediments, as well as hydrogenous Mn oxides, owing to their high concentrations of transition metals (Arrhenius et al., 1957; Bernat, 1975; Kashiwabara et al., 2014, 2018; Machida et al., 2016; Takaya et al., 2018; Toyoda et al., 1990; Yasukawa et al., 2016), both of which were commonly observed in the REY-rich mud in microscopic observations (Ohta et al., 2016, 2020).

5.2.2.1. Proportions of BCP

The samples with relatively low Sr isotopic ratios—Units II, III, and IV and the REY peaks—may have been more affected than Unit I by components other than terrigenous materials. Their PAAS-normalized REY patterns show a clear negative Ce anomaly and enrichment in middle to heavy rare-earth elements (Figure S2 in Supporting Information S1; Fujinaga et al., 2016; Iijima et al., 2016; Tanaka, Nakamura, Yasukawa, Mimura, Fujinaga, Iijima et al., 2020). These features resemble those of BCP represented by fish teeth and bone fragments in deep-sea sediments (Takaya et al., 2018; Toyoda et al., 1990). Moreover, these samples are categorized as REY-rich mud, that is, sediments with $\Sigma\text{REY} > 400$ ppm (Kato et al., 2011; Tanaka, Nakamura, Yasukawa, Mimura, Fujinaga, Iijima et al., 2020), and contain several percent to 30% BCP according to microscopic observations (Ohta et al., 2016). Therefore, the addition of fish teeth (BCP) with relatively low Sr isotopic ratios ($^{87}\text{Sr}/^{86}\text{Sr} = 0.707854\text{--}0.709123$; Section 4.2) can explain the lower $^{87}\text{Sr}/^{86}\text{Sr}$ values in bulk REY-rich mud compared to those of Unit I.

The proportion of BCP in the bulk sediment samples was estimated by considering the mixing between the terrigenous component and BCP. For the estimation, we used the P_2O_5 content as an indicator of BCP. The BCP in deep-sea sediments in the study area contains 29.8 wt.% P_2O_5 on average (Table S5 in Supporting Information S2; Takaya et al., 2018). In contrast, the terrigenous component (e.g., Chinese Loess) and Mn nodules of mainly hydrogenous origin that were collected ~300 km east of Minamitorishima Island (hereafter referred to as Minamitorishima Mn nodules) contain ~0.15 wt.% and ~0.99 wt.% P_2O_5 , respectively (Table S5 in Supporting Information S2; Gallet et al., 1996; Fujinaga et al., 2016; Machida et al., 2016). The effects of organic-derived phosphorous could be considered to be negligible because organic matter was not confirmed by smear slide observations (Ohta et al., 2016, 2020). Indeed, sediment samples collected in the same area generally contain less than 0.1 wt.% total organic carbon (i.e., the core at ~14 km northwest of KR13-02 PC05; Y. Usui et al., 2017). Therefore, almost all of the phosphorous content in the samples can be considered to originate from BCP.

The estimation method is described in Text S2 in Supporting Information S1. The estimated proportions of BCP for each sample are shown in Table 1. The BCP proportion in Unit I is very low (<1%), whereas those of Units II to V and the REY peaks are greater than 1%. Notably, the REY peak samples have the largest proportions of BCP, ranging between 12% and 33%. The proportions of BCP in Units II, III, and V range between 1.5% and 5%, except for two samples, whereas those in Unit IV are relatively high (5%–12%).

Notably, the bulk chemical compositions of Units II to V reflect the BCP input. In addition to phosphorous, CaO, Th, U, and REY are enriched in BCP (Arrhenius et al., 1957; Toyoda et al., 1990; Trueman & Tuross, 2002). The depth profiles of CaO, Th, U, and REY contents in Cores KR13-02 PC04 and PC05 (Figure 5; Iijima et al., 2016;

Table 1
Estimated Proportions of Biogenic Calcium Phosphate (BCP) and Hydrogenous Mn Oxides Based on the Method Described in Text S2 in Supporting Information S1

Cruise	PC	Sec-tion	Top [cm]	Bottom [cm]	Depth [mbsf]	ΣREY [ppm]	⁸⁷ Sr/ ⁸⁶ Sr	BCP [%]	Hydrogenous Mn-oxides [%]	Chemostrati-graphic unit ^a	Reference (Sr isotope)
KR13-02	4	2	32	34	0.85	333	0.713370	0.5	1.5	Unit I	This study
KR13-02	4	3	52	54	2.06	454	0.711605	1.0	2.0	Unit II	Yasukawa et al. (2019)
KR13-02	4	8	52	54	7.00	638	0.708960	2.0	3.5		Yasukawa et al. (2019)
KR13-02	4	9	82	84	8.29	4,968	0.708918	24	5.5	1st REY peak	Yasukawa et al. (2019)
KR13-02	4	9	92	94	8.39	4,542	0.709042	24	5.0		Yasukawa et al. (2019)
KR13-02	4	10	42	44	8.97	1,422	0.710710	9.0	4.5	Unit IV	Yasukawa et al. (2019)
KR13-02	4	11	82	84	10.37	1,800	0.710310	11	4.5		Yasukawa et al. (2019)
KR13-02	4	12	42	44	10.97	1,777	0.710194	12	5.0		Yasukawa et al. (2019)
KR13-02	5	1	2	4	0.03	363	0.713645	0.5	2.0	Unit I	This study
KR13-02	5	1	12	14	0.13	312	0.714183	0.5	1.5		This study
KR13-02	5	2	42	44	0.70	0.00	0.709782	2.0	4.0	Unit II	This study
KR13-02	5	2	82	84	1.10	453	0.709449	1.5	2.5		This study
KR13-02	5	3	22	24	1.50	659	0.709239	2.5	5.0		This study
KR13-02	5	3	32	34	1.60	590	0.709196	2.5	4.0		Yasukawa et al. (2019)
KR13-02	5	3	82	84	2.10	796	0.708895	3.5	4.0		This study
KR13-02	5	4	12	14	2.37	1,206	0.709109	5.5	4.0		Yasukawa et al. (2019)
KR13-02	5	4	22	24	2.47	1,553	0.709062	7.0	4.5		This study
KR13-02	5	4	62	64	2.87	4,402	0.708820	21	5.0	1st REY peak	Yasukawa et al. (2019)
KR13-02	5	4	72	74	2.97	6,799	0.708717	32	3.5		This study
KR13-02	5	4	92	94	3.17	5,955	0.708715	33	3.0		This study
KR13-02	5	5	22	24	3.47	3,937	0.709011	23	3.5		This study
KR13-02	5	5	22	24	3.47	3,937	0.709001	23	3.5		This study
KR13-02	5	5	72	74	3.97	1,057	0.712489	4.5	4.0	Unit III	This study
KR13-02	5	5	92	94	4.17	950	0.712105	4.0	3.5		This study
KR13-02	5	6	72	74	4.97	984	0.711834	4.0	4.0		This study
KR13-02	5	6	82	84	5.07	1,019	0.711778	4.0	4.0		This study
KR13-02	5	7	72	74	5.97	557	0.710907	2.5	3.5		This study
KR13-02	5	7	82	84	6.07	795	0.711505	2.5	3.5		Yasukawa et al. (2019)
KR13-02	5	8	52	54	6.77	2,485	0.709885	14	4.0	2nd REY peak	This study
KR13-02	5	8	72	74	6.97	2,026	0.709702	17	3.5		This study
KR13-02	5	9	72	74	7.96	1,120	0.709642	10	3.0	Unit IV	This study
KR13-02	5	9	72	74	7.96	1,120	0.709650	10	3.0		Yasukawa et al. (2019)
KR13-02	5	10	32	34	8.56	989	0.711637	5.5	2.5		This study
KR13-02	5	10	72	74	8.96	972	0.711844	4.5	2.0	Unit V	This study
KR13-02	5	10	82	84	9.06	976	0.711975	4.0	2.5		This study
KR13-02	5	11	82	84	10.05	1,055	0.711724	3.5	3.5		This study
KR13-02	5	12	82	84	11.05	1,041	0.713033	3.5	3.5		Yasukawa et al. (2019)
KR13-02	6	7	92	94	6.49	2,564	0.709555	12	4.5	2nd REY peak	This study
KR13-02	6	8	2	4	6.59	3,341	0.709467	16	4.5		This study
KR13-02	6	8	12	14	6.69	4,656	0.709235	23	5		This study
KR13-02	PCPL04	1	0	2	0.01	267	0.712774	0.5	1.5	Unit I	This study
KR13-02	PCPL04	1	3	5	0.04	281	0.712858	0.5	1.5		This study

Table 1
Continued

Cruise	PC	Sec-tion	Top [cm]	Bottom [cm]	Depth [mbsf]	ΣREY [ppm]	⁸⁷ Sr/ ⁸⁶ Sr	BCP [%]	Hydrogenous Mn-oxides [%]	Chemostrati-graphic unit ^a	Reference (Sr isotope)
MR13-E02	1	1	54	56	0.55	243	0.713401	0	1	Unit I	This study
MR13-E02	3	1	54	56	0.55	173	0.713814	0	0.6		Yasukawa et al. (2019)
MR13-E02	3	8	44	46	7.05	183	0.712965	0	0.7		Yasukawa et al. (2019)
MR13-E02	3	9	94	96	8.55	203	0.711866	0	0.9		Yasukawa et al. (2019)
MR13-E02	3	14	44	46	13.06	204	0.713870	0	0.9		Yasukawa et al. (2019)
MR14-E02	5	9	54	56	7.77	2,406	0.709869	14	3.5	2nd REY peak	Yasukawa et al. (2019)
MR14-E02	5	10	8	10	8.32	2,368	0.709911	16	3.5		Yasukawa et al. (2019)
MR14-E02	5	10	54	56	8.78	2,266	0.709977	15	3.5		Yasukawa et al. (2019)
MR14-E02	8	7	54	56	6.44	5,570	0.709183	26	3.5	2nd REY peak	Yasukawa et al. (2019)
MR14-E02	8	9	4	6	7.92	1,469	0.711206	7	4	Unit V	Yasukawa et al. (2019)
MR14-E02	9	1	54	56	0.55	352	0.713384	0.5	2	Unit I	Yasukawa et al. (2019)
MR14-E02	9	7	4	6	5.80	3,683	0.709215	18	4	1st REY peak	Yasukawa et al. (2019)
MR14-E02	9	7	54	56	6.30	2,887	0.709505	14	4		Yasukawa et al. (2019)
MR14-E02	9	8	4	6	6.80	1,131	0.711242	5	4.5	Unit II	Yasukawa et al. (2019)
MR14-E02	PCPL04	1	0	2	0.01	295	0.713833	0.5	1.5	Unit I	This study
MR14-E02	PCPL05	1	0	2	0.01	294	0.713355	0.5	1.5		This study
MR14-E02	PCPL08	1	0	2	0.01	293	0.713382	0.5	1.5		This study
MR14-E02	PCPL09	1	0	2	0.01	285	0.713382	0.5	1.5		This study
MR14-E02	PCPL11	1	0	2	0.01	273	0.713586	0.5	1.5		This study
MR15-E01	2	10	92	94	9.87	578	0.716030	1.5	1.5	Unit V	This study
MR15-E01	2	11	92	94	10.87	660	0.714767	2	2		This study
MR15-E01	2	12	92	94	11.87	628	0.714424	2	2		This study
MR15-E01	2	13	26	28	12.22	407	0.716845	1.5	0		This study

^aThe chemostratigraphic unit classification is based on the method described by Tanaka, Nakamura, Yasukawa, Mimura, Fujinaga, Iijima et al. (2020).

this study) are almost identical to those of P₂O₅ content. In addition, they resemble the depth profile of the estimated proportions of BCP in Cores KR13-02 PC04 and PC05 (Table 1), which supports the validity of our estimation. This result also implies that REY, Th, and U contents, which are widely used in the discussion of petrological characteristics, could be less useful for the sediments rich in BCP.

5.2.2.2. Proportions of Hydrogenous Mn Oxides

Another material that may lead to a decrease in the ⁸⁷Sr/⁸⁶Sr ratio of bulk sediment is hydrogenous Mn oxides. Dubinin et al. (2017) reported that the ⁸⁷Sr/⁸⁶Sr of Mn micronodules in sediments from the Brazil basin in the Atlantic Ocean is similar to that of modern seawater; thus, they proposed that Sr exchange has occurred between the micronodules and ambient pore water/seawater. Yasukawa et al. (2020) estimated that the major portion (50%–90%) of Fe–Mn (oxyhydr)oxides in the REY-rich mud around Minamitorishima Island is in the form of hydrogenous Mn microparticles, which were originally reported in the South Pacific pelagic clay (Uramoto et al., 2019). Considering that the leachate of macroscopic Mn nodules of hydrogenous origin showed modern seawater-like values (⁸⁷Sr/⁸⁶Sr = 0.709096–0.709181) regardless of the sampling position (i.e., in both the surface and inner layers of the nodules), the exchange of Sr with seawater could be a common phenomenon in both macroscopic Mn nodules on the seafloor and Mn microparticles in the sediment. Therefore, the hydrogenous Mn oxides in the REY-rich mud could affect the Sr isotopic composition of the bulk sediments.

The proportion of hydrogenous Mn oxides in each bulk sediment sample was estimated by considering the mixing between the terrigenous component and hydrogenous Mn oxides. For the estimation, we used the Co content as an indicator of hydrogenous Mn oxides. Zhou and Kyte (1992) suggested that Co precipitates slowly at a constant

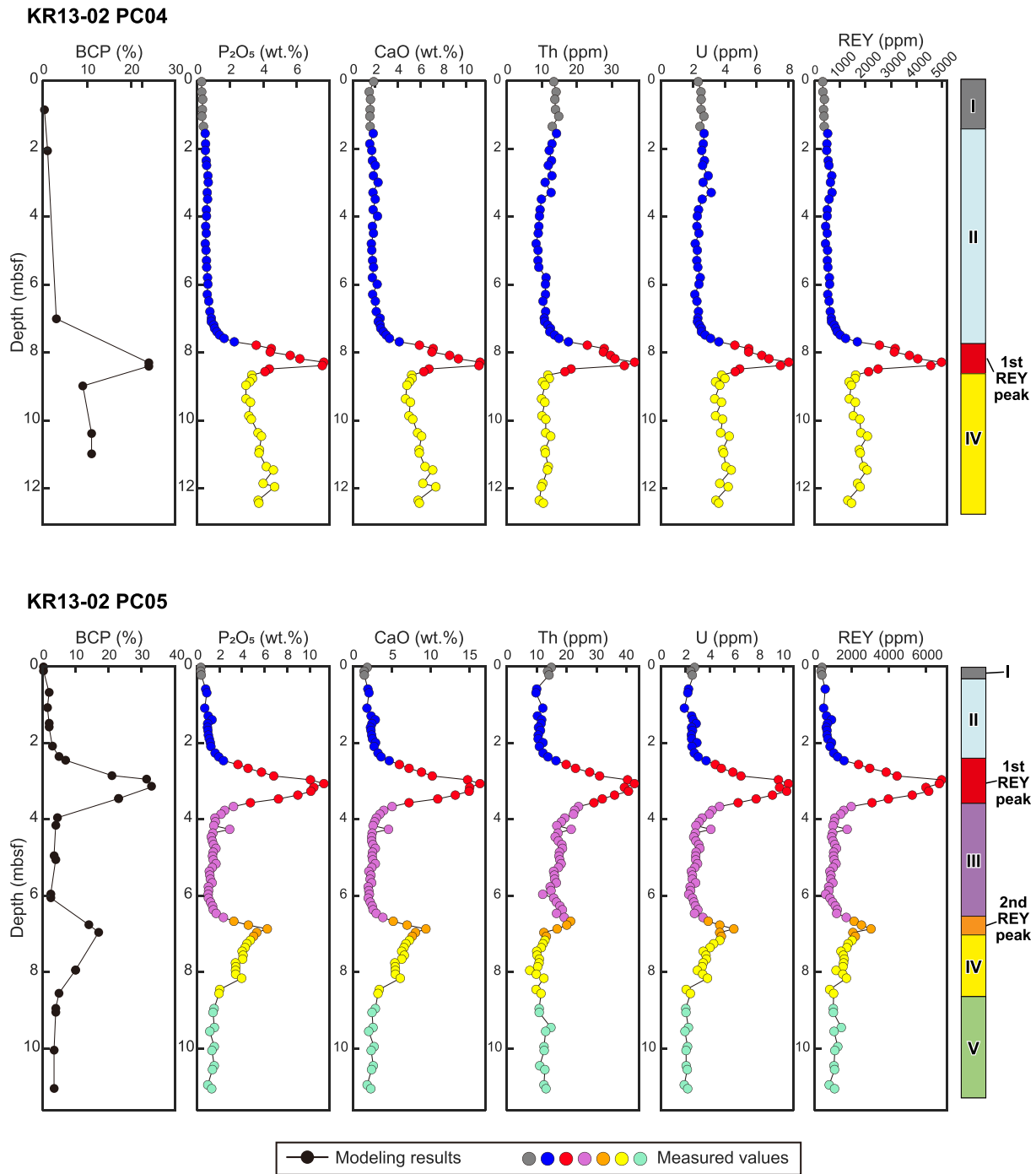


Figure 5. Depth profiles of the estimated proportions of biogenic calcium phosphate (this study), and measured P_2O_5 , CaO, Th, U, and rare earth elements and yttrium contents (Iijima et al., 2016; this study) with chemostratigraphic units (Tanaka, Nakamura, Yasukawa, Mimura, Fujinaga, Iijima et al., 2020) of Cores KR13-02 PC04 and PC05.

rate from seawater; thus, many studies employ the Co flux to measure the depositional age of pelagic clays (e.g., Dunlea, Murray, Sauvage, Pockalny, et al., 2015; Kyte et al., 1993; Zhou & Kyte, 1992). The terrigenous component (e.g., Chinese Loess) and BCP demonstrate Co contents of ~ 8.7 and ~ 5 ppm, respectively (Table S5 in Supporting Information S2; Fujinaga et al., 2016; Sun & Zhu, 2010; Takaya et al., 2018). In contrast, the Minamitorishima Mn nodules exhibit Co contents of $\sim 4,400$ ppm (Table S5 in Supporting Information S2;

Machida et al., 2016). Therefore, most of the Co content in the bulk sediment could have been derived from the hydrogenous Mn oxides by slow precipitation.

The proportion of hydrogenous Mn oxides in Unit I is less than 2% (Table 1), as determined by the estimation method described in Text S2 in Supporting Information S1. In contrast, most of the samples from Units II to V and the REY peaks are enriched in Co and hydrogenous Mn oxides, with contents of 2%–5.5% (Table 1). It is notable that three samples in MR15-E01 PC02 show relatively low REY contents ($\Sigma\text{REY} = 410\text{--}660$ ppm; Table S2 in Supporting Information S2), suggesting that they contain less BCP compared to the other samples. Therefore, the negative Ce anomaly of BCP could be partly offset by hydrogenous Mn-oxides, resulting in the smaller negative Ce anomaly in the PAAS-normalized REY patterns of bulk sediments (see Section 4.1, Figure S2 in Supporting Information S1).

Figure 6 shows the depth profiles of Co, MnO, and Ni contents of Cores KR13-02 PC04 and PC05 (Iijima et al., 2016; this study), and those of the proportions of Mn-oxides (Table 1). The depth profiles of the MnO and Ni contents in Cores KR13-02 PC04 and PC05 resemble those of the Co contents and estimated Mn-oxide proportions; that is, the increasing trends from Unit I to the 1st REY peak and from the bottom of Unit III to 2nd REY peak, the maximum value in the 1st REY peak, the decreasing trend in Unit IV, and the minimum value from the bottom of Unit IV to Unit V. MnO and Ni are also incorporated into the Mn-oxide phase regardless of its size; that is, macro-nodules, Fe-Mn micronodules, and microparticles (Hein & Koschinsky, 2014; Uramoto et al., 2019; Yasukawa et al., 2020). These consistent features in the depth profiles imply that the proportions of Mn-oxides were estimated properly.

5.3. Mixture Models of End-Member Components Based on Bulk Sediment Sr Isotopic Ratios

5.3.1. Model 1: Terrigenous Component + BCP + Mn Oxides

A model calculation is introduced to reproduce the observed depth profiles of the bulk Sr isotopic ratios, as shown in Figure 4. Considering the observed geochemical features discussed in Section 5.2, we first considered a model of three-component mixing of the terrigenous component, BCP, and hydrogenous Mn oxides (Table 2), which were labeled as Model 1. This ternary mixing model is consistent with the result of independent component analysis by Yasukawa et al. (2019), although the data set statistically analyzed ($n = 567$) was merely a part of the entire data set in the study area (totally $n = 1,685$, including the above 567 samples; Tanaka, Nakamura, Yasukawa, Mimura, Fujinaga, Iijima et al., 2020; Tanaka, Nakamura, Yasukawa, Mimura, Fujinaga, Ohta et al., 2020). The calculation methods are based on those reported by Langmuir et al. (1978), Holland (1984), and Palmer and Elderfield (1985), details of which are provided in Text S3 in Supporting Information S1. Table S5 in Supporting Information S2 shows representative compositions of the potential end-member components used in the model calculation.

Model 1 can reproduce a major portion of the measured $^{87}\text{Sr}/^{86}\text{Sr}$ ratio (Figure 7b). The exceptions are the intervals at Unit II and the 1st REY peak, and Units III and IV. In these intervals, the calculated $^{87}\text{Sr}/^{86}\text{Sr}$ values are higher than the observed values. This discrepancy suggests that other end-member(s) with low $^{87}\text{Sr}/^{86}\text{Sr}$ are present in these intervals and that a three-component mixing model is insufficient to explain the $^{87}\text{Sr}/^{86}\text{Sr}$ ratios of the bulk sediments.

5.3.2. Volcanic Components as Additional End-Member Components

Model 1 requires the addition of components with low $^{87}\text{Sr}/^{86}\text{Sr}$ ratios between Unit II and the 1st REY peak and in Unit IV. One possible component with low $^{87}\text{Sr}/^{86}\text{Sr}$ ratios is a volcanic material. Table S5 in Supporting Information S2 lists the average $^{87}\text{Sr}/^{86}\text{Sr}$ values of fresh mid-ocean ridge basalt lava (MORB; global average), lavas from the WPSP and petit-spot volcanos, and tephra from the Mariana and Izu-Bonin arc, which generally have $^{87}\text{Sr}/^{86}\text{Sr}$ values below 0.7050 (Gale et al., 2013; Koppers et al., 2003; Machida et al., 2009; Miyazaki et al., 2015; Savov et al., 2006; Straub et al., 2010, 2015, 2017; White & Klein, 2014). Previous studies have not discussed any notable enrichment of volcanic components in the study area on the basis of the chemical compositions of the bulk sediments (Fujinaga et al., 2016; Iijima et al., 2016; Yasukawa et al., 2019). Regarding the statistical analysis reported by Yasukawa et al. (2019), this is probably because only a limited number of elements were used (i.e., major elements, REY, Co, Ni, and Cu). However, Asahara (1999) and Asahara et al. (1999) reported that a volcanic component was supplied to the sediment in the area around Minamitorishima Island. In addition,

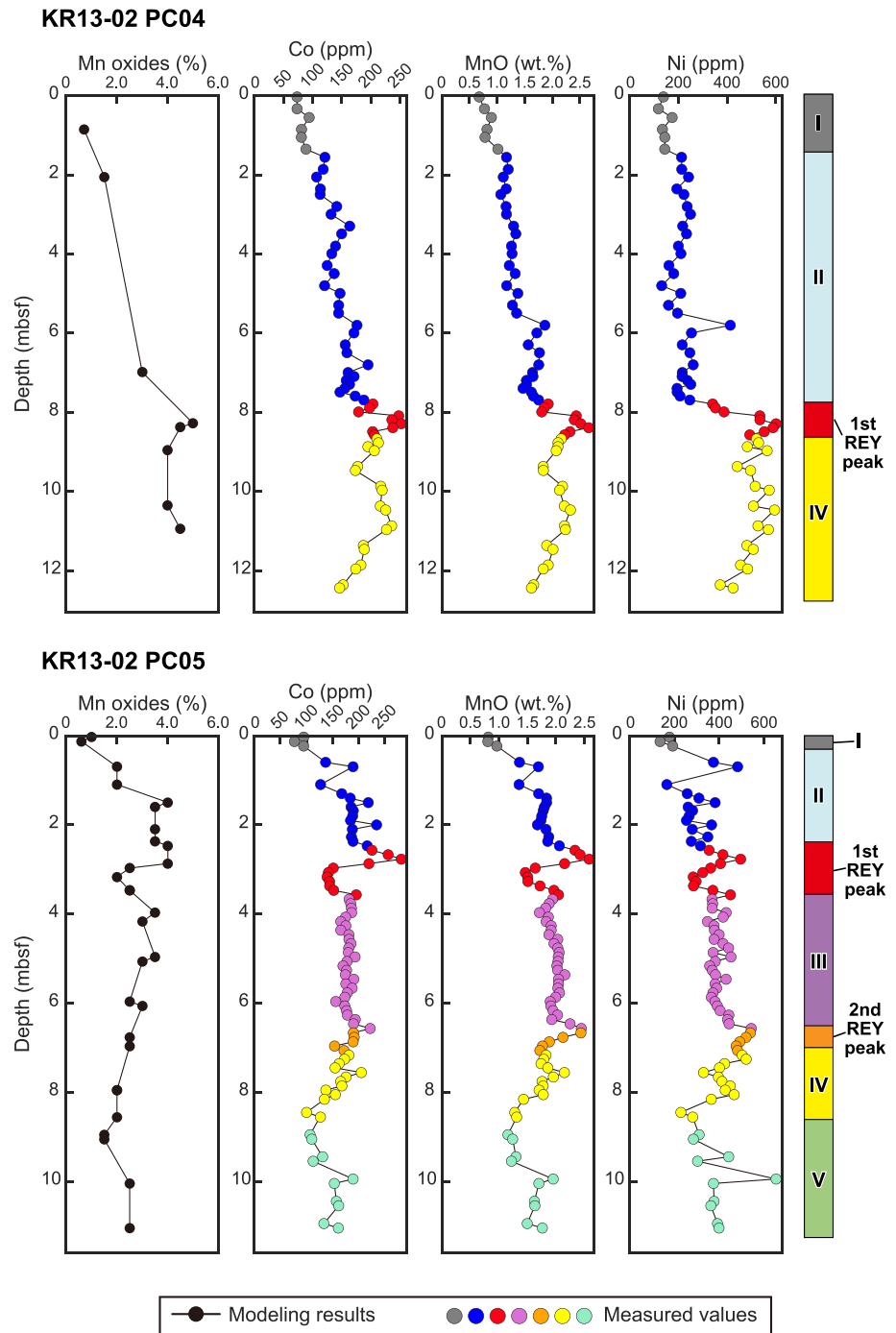


Figure 6. Depth profiles of the estimated proportions of hydrogenous Mn oxides (this study), and measured Co, MnO, and Ni contents (Iijima et al., 2016; this study) with chemostratigraphic units (Tanaka, Nakamura, Yasukawa, Mimura, Fujinaga, Iijima et al., 2020) of Cores KR13-02 PC04 and PC05.

Ohta et al. (2016) reported zeolite-rich intervals in KR13-02 PC05: 0.5 to 2.7 mbsf and 7.9 mbsf to the bottom of the core (Unit II to the 1st REY peak, and Units IV to V). These intervals are generally classified as zeolitic clay or clay with zeolite, owing to the presence of 10%–30% phillipsite according to smear slide observations (*cf.* Section 3). Phillipsite has been considered to form during early diagenesis of volcanic glass under conditions with a low sedimentation rate (Bernat & Goldberg, 1968; Bernat et al., 1970; Czyscinski, 1973; Stonecipher, 1976). It is notable that phillipsite shows low Sr concentrations (<35 ppm; Takaya et al., 2018), suggesting an elution of

Table 2
End-Member Components Used in the Model Calculations

Model	Components
1	Terrigenous component + BCP + Mn oxides
2	Terrigenous component + BCP + Mn oxides + MORB
3	Terrigenous component + BCP + Mn oxides + Lavas from WPSP
4	Terrigenous component + BCP + Mn oxides + Petit-spot lavas
5	Terrigenous component + BCP + Mn oxides + Tephra from the Mariana arc
6	Terrigenous component + BCP + Mn oxides + Tephra from Izu-Bonin arc

Sr from volcanic materials during crystallization or alteration to form phillipsite. However, if the eluted volcanic Sr has been retained in the surrounding sediments, the bulk Sr contents and isotope ratios would not be affected by such an event of alteration/crystallization.

Thus, we take into account the effects of phillipsite as a volcanic material to test this assumption. Models 2–6 represent the mixing of the terrigenous component, BCP, hydrogenous Mn oxide, and a volcanic component from the MORB, WPSP, petit-spot volcanos, and the Mariana and Izu-Bonin arcs, respectively (Figures 7c–7g, Table S5 in Supporting Information S2; Bryant et al., 2003; Christie et al., 1995; Gale et al., 2013; Koppers et al., 2003; Machida et al., 2009; Miyazaki et al., 2015; Savov et al., 2006; Straub et al., 2010, 2015, 2017; White & Klein, 2014). The observed modal composition of phillipsite in each sample, obtained by smear slide observations, was applied as the abundance of volcanic components (Ohta et al., 2016, 2020; Table S7 in Supporting Information S2). For the Mariana and Izu-Bonin arcs, only tephra records between 40 and 23 Ma were applied because they formed mature arcs before the cessation of the Izu-Bonin volcanism in the Oligocene (Brandl et al., 2017; Johnson et al., 2021; Shipboard Scientific Party, 2002).

5.3.2.1. Model 2: Terrigenous Component + BCP + Mn Oxides + MORB

Model 2 is based on the assumption that MORB (Gale et al., 2013; White & Klein, 2014) is a volcanic end-member (Table 2). The calculated $^{87}\text{Sr}/^{86}\text{Sr}$ values using Model 2, as shown in Figure 7c, are similar to the measured values at ~8 mbsf, or Unit IV. As a result, the addition of MORB results in better fitting of the 2nd REY peak to Unit IV compared to Model 1, although the calculated values remain higher than the measured values of Unit II.

5.3.2.2. Model 3: Terrigenous Component + BCP + Mn Oxides + Lavas From WPSP

The WPSP was active during the Cretaceous, from approximately 140 to 70 Ma (Christie et al., 1995; Koppers et al., 2003). In addition, the boundary of the pelagic clay and chert around Minamitorishima Island is reportedly late Campanian (Shipboard Scientific Party, 1990). The depositional age of the pelagic clay around Minamitorishima Island suggests that the WPSP may affect the lowermost part of the piston core. Based on the calculation, the measured $^{87}\text{Sr}/^{86}\text{Sr}$ values are in the range of the $^{87}\text{Sr}/^{86}\text{Sr}$ values of Model 3 throughout the core (Figure 7d). Thus, the WPSP might be a possible source of volcanic materials on the basis of the Sr isotope modeling.

5.3.2.3. Model 4: Terrigenous Component + BCP + Mn Oxides + Lavas From Petit-Spot Volcanos

Petit-spot volcanos are also among the closest sources of volcanic material in the area around Minamitorishima Island (e.g., Hirano et al., 2019), although the reported ages of petit-spot volcanos around Minamitorishima Island are markedly younger (<3 Ma; Hirano et al., 2019) than the onset of Unit II deposition (Nozaki et al., 2019; Ohta et al., 2020; Usui & Yamazaki, 2021). Model 4 considers the mixing of the terrigenous component, BCP, hydrogenous Mn oxides, and petit-spot basalt (Table 2). It yields similar Sr isotopic values to the sample data in Units II and IV, as in the case of Model 3 (Figure 7e); thus, petit-spot volcanos could be another possible source of the volcanic material in the sediments.

5.3.2.4. Models 5 and 6: Terrigenous Component + BCP + Mn Oxides + Tephra From the Mariana and Izu-Bonin Arcs

In Models 5 and 6, we applied the isotopic and elemental values of tephra layers from the Mariana and Izu-Bonin arcs, respectively (Bryant et al., 2003; Savov et al., 2006; Straub et al., 2010, 2015, 2017) as volcanic end-members (Table 2). Models 5 and 6, which consider the effects of tephra supply from the Mariana and Izu-Bonin arcs, show

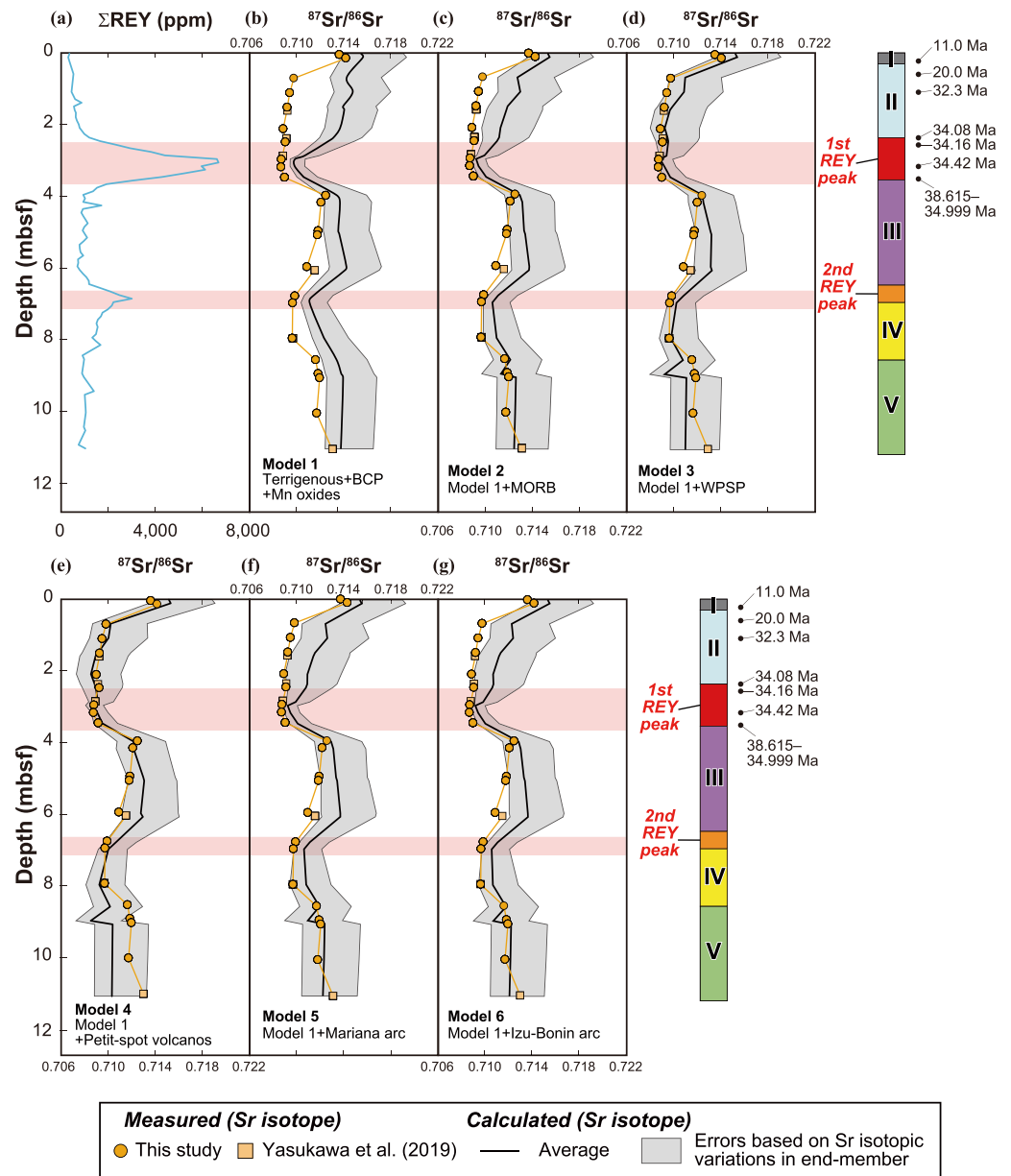


Figure 7. Depth profiles of (a) total rare earth elements and yttrium (REY) content and (b)–(g) comparison of the calculated $^{87}\text{Sr}/^{86}\text{Sr}$ values from Models 1–6 with the measured $^{87}\text{Sr}/^{86}\text{Sr}$ values of KR13-02 PC05. In (b)–(g), the measured values are shown in orange whereas the calculated values are in black. The gray shading indicates errors based on the Sr isotopic variation in the end-members. The REY peaks are indicated by horizontal pink bars. (b) Model 1 shows the mixing of the Chinese Loess (Chen et al., 2007; Gallet et al., 1996; Jahn et al., 2001; Taylor et al., 1983; Yokoo et al., 2004), biogenic calcium phosphate (Takaya et al., 2018; this study), and Mn oxides (Machida et al., 2016; this study), whereas (c)–(g) Model 2 to Model 6 consider the mixing of the three components in Model 1 along with a volcanic component. The applied values of the volcanic components are average values of (c) MORB (global average; Gale et al., 2013; White & Klein, 2014), (d) lavas from West Pacific Seamount Province (Christie et al., 1995; Koppers et al., 2003), (e) petit-spot lavas (Machida et al., 2009; Miyazaki et al., 2015), (f) tephra from the Mariana arc (Bryant et al., 2003; Straub et al., 2015, 2017), and (g) tephra from the Izu-Bonin arc (Savov et al., 2006; Straub et al., 2010). The chemostratigraphic classification is from Tanaka, Nakamura, Yasukawa, Mimura, Fujinaga, Iijima et al. (2020), and the depositional ages are from Ohta et al. (2020).

slightly higher $^{87}\text{Sr}/^{86}\text{Sr}$ values (Figures 7f and 7g). However, their curves can explain the observed $^{87}\text{Sr}/^{86}\text{Sr}$ in Unit II and the 1st REY peak better than those of Model 1 in Unit II and the 1st REY peak. This result implies the possibility that the Minamitorishima sediments of Unit II and the 1st REY peak could contain the Izu-Bonin-Mariana tephra.

5.3.3. Constraints of the Volcanic End-Member Sources Based on the Bulk Chemical and Mineralogical Compositions With Sr Isotope Ratios

The model calculations in Section 5.3.2 support the possibility that the input of volcanic materials, such as MORB, lavas from WPSP and petit-spot volcanos, and tephra from the Mariana and Izu-Bonin arcs (40–23 Ma), could lower the bulk $^{87}\text{Sr}/^{86}\text{Sr}$ isotope values at Unit II, the 1st REY peak, and Unit IV. In addition, they suggest that phillipsite could be useful for estimating the proportions of volcanic materials, even though strontium could have been eluted during phillipsite crystallization or alteration of the original volcanic materials. To strongly test the Sr modeling results, this section discusses the source of the terrigenous and volcanic materials based on the bulk chemical and mineralogical compositions, in addition to the $^{87}\text{Sr}/^{86}\text{Sr}$ values. The discussion in this section includes the $^{87}\text{Sr}/^{86}\text{Sr}$ ratios not only reported in this study (Table S2 in Supporting Information S2), but also reported by Yasukawa et al. (2019), that is, samples from KR13-02 PC04 and PC05, MR13-E02 PC03, and MR14-E02 PC05 and PC08 (Table 1). Furthermore, to expand the data set and to discuss the variation among the units, the scatter diagrams in this section include all chemical compositional data obtained from all eight piston and six pilot cores (KR13-02 PC04, PC05, and PC06, MR13-E02 PC01 and PC03, MR14-E02 PC05 and PC08, MR15-E01 PC02, KR13-02 PCPL04, and MR14-E02 PCPL04, PCPL05, PCPL08, PCPL09, and PCPL11); this study and Yasukawa et al. (2019) reported the collection of one or more samples from the cores for Sr isotope analyses. They are from Fujinaga et al. (2016), Iijima et al. (2016), Takaya et al. (2018), Yasukawa et al. (2019), Tanaka, Nakamura, Yasukawa, Mimura, Fujinaga, Iijima et al. (2020), and this study.

The proportional changes in the terrigenous and volcanic components can be observed in the depth profiles of Rb, Cs, and Ba contents in KR13-02 PC04 and PC05 (Figure 8). Previous studies reported that Rb, Cs, and Ba content values are high in continental materials, but are low in volcanic materials (Dunlea, Murray, Sauvage, Spivack, et al., 2015; Plank & Langmuir, 1998). Figure 8 shows that Unit II, the 1st REY peak, and Unit IV contain less than 100 ppm of Rb, 7.5 ppm of Cs, and 400 ppm of Ba. This strongly suggests that the proportions of the volcanic materials in Unit II, the 1st REY peak, and Unit IV are greater than those in continental materials. In other words, Units I and III, which show high Rb and Cs contents, are dominated by the input of continental materials. This is supported by the observation that the estimated proportion of terrigenous materials exhibits a depth profile similar to that of the Rb and Cs content values in KR13-02 PC04 and PC05 (Figure 8). The characteristics of Unit V are different from those of Units I and III; Unit V shows high Rb (approximately 100 ppm) but low Cs (less than 7.5 ppm), which will be discussed in Section 5.4.3.

The La/Yb ratio and Th content of bulk sediments provide another constraint for the provenance of the volcanic materials in Unit II (Figures 9a and S3 in Supporting Information S1). Since, Th is incorporated into BCP (*cf.* Section 5.2.2.1), the 1st and 2nd REY peaks exhibit Th enrichment around La/Yb = ~ 6 –7. On the other hand, Unit I sediments, which are mainly derived from terrigenous components, show a trend toward Chinese Loess in Figure 9a. Although Units III and V are located in the mixing trend between BCP and Chinese Loess (or between the REY peaks and Unit I), Unit II deviates from the mixing trend due to lower La/Yb ratios than those of BCP and Chinese Loess and shifts toward the Izu-Bonin and Mariana tephtras or MORB, rather than the lavas from WPSP or petit-spot volcanos.

In addition to the scatter diagram of La/Yb and Th, the relationship between $1/\text{Sr}$ and $^{87}\text{Sr}/^{86}\text{Sr}$ (Figure 9b) suggests the provenance of the volcanic components. On the $1/\text{Sr}$ – $^{87}\text{Sr}/^{86}\text{Sr}$ diagram, the mixing between any two components can be illustrated as a straight line. The Sr contents of most samples from Units I, III, and V are in the range of the Chinese Loess (approximately $1/\text{Sr} = 0.003$ – 0.012), whereas the 1st and 2nd REY peaks in Figure 9b exhibit a trend toward the BCP with $1/\text{Sr} = 0.00071$ and $^{87}\text{Sr}/^{86}\text{Sr} = 0.7079$ – 0.7091 (Table S5 in Supporting Information S2). Although they are on the mixing trend between Chinese Loess and BCP, the other samples (*i.e.*, the Units II samples in blue dashed circle in Figure 9b) are not located between Unit I and the REY peaks due to low $^{87}\text{Sr}/^{86}\text{Sr}$ values. Considering the $1/\text{Sr}$ values of the volcanic materials (Figure 9b), the Unit II samples shift toward the Izu-Bonin and Mariana tephtras or MORB, which are distinguishable from the lavas from petit-spot volcanos and from WPSP. Moreover, Th/La and Nb/La ratios of Unit II (Figure 9c) are extremely close to the ranges of the Izu-Bonin and Mariana tephtras, whereas the Nb/La ratios of Unit II are clearly lower than those of MORB, lavas from petit-spot volcanos, and WPSP. Thus, the low Sr isotope ratios of Unit II are attributed to the tephra input from the Izu-Bonin and Mariana arcs. The modeling results of four-component mixing (Chinese Loess + BCP + hydrogenous Mn-oxides + tephra from the Izu-Bonin arc) on Rb and Ba contents are also shown in Figure 8. Their depth profiles generally mimic the measured values: relatively high in Units I and III and low

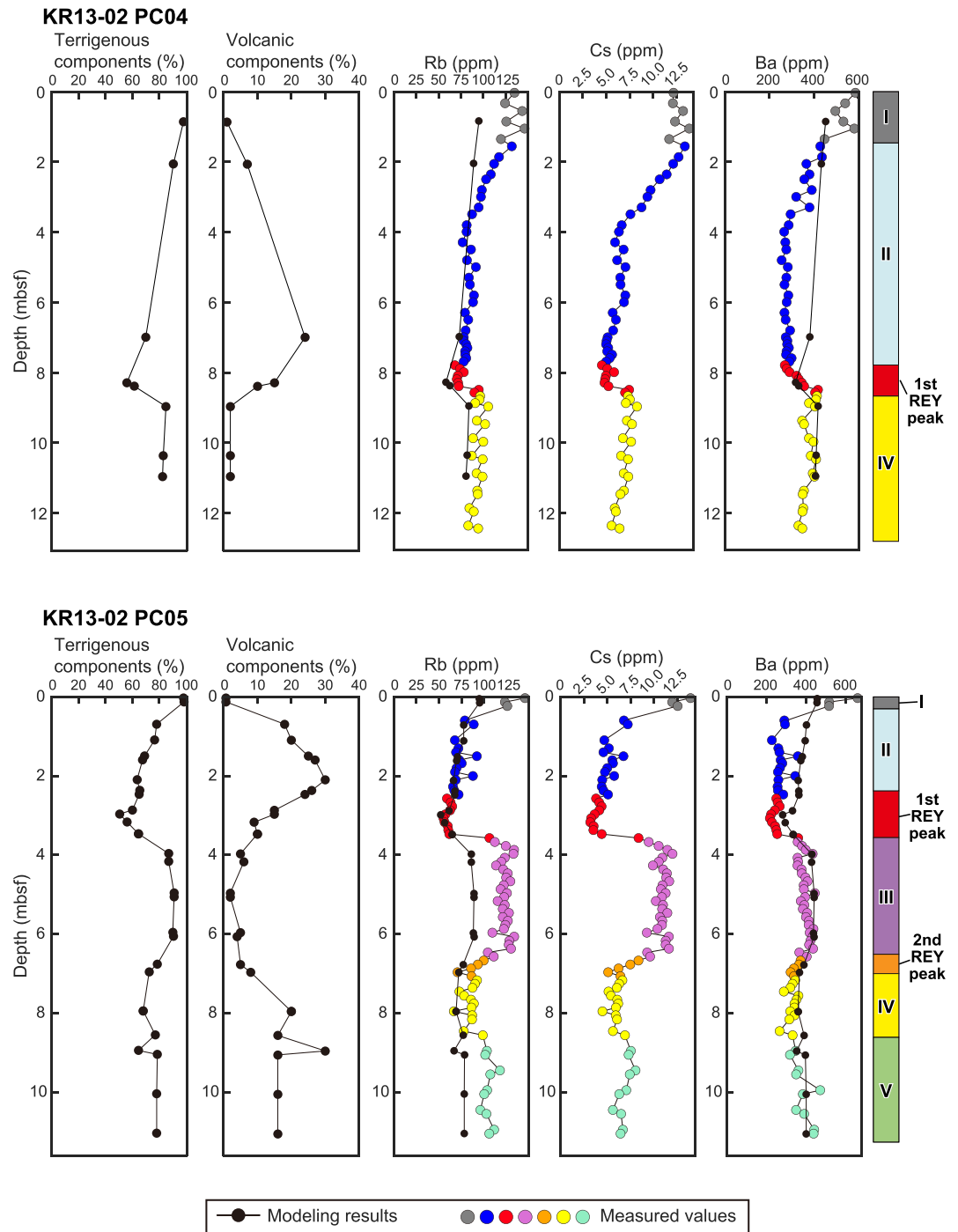


Figure 8. Depth profiles of the estimated proportions of terrigenous and volcanic components (this study), and measured Rb, Cs, and Ba contents (Iijima et al., 2016; Tanaka, Nakamura, Yasukawa, Mimura, Fujinaga, Iijima et al., 2020; this study) with chemostratigraphic units (Tanaka, Nakamura, Yasukawa, Mimura, Fujinaga, Iijima et al., 2020) of Cores KR13-02 PC04 and PC05. Regarding Rb and Ba contents, the mixing modeling results of four-components (i.e., Chinese Loess, biogenic calcium phosphate, hydrogenous Mn-oxides, and tephra from Izu-Bonin arc) are shown by black dots and curves.

in Units II and IV. In addition to Sr isotopes, the consistent patterns of different elemental contents further support the input of the tephra from the Izu-Bonin and Mariana arcs. However, the calculated Rb and Ba contents are lower than the measured values in Units III and Unit II, respectively. This implies that the chemical compositions of terrigenous or volcanic endmembers could be more variable than our assumption.

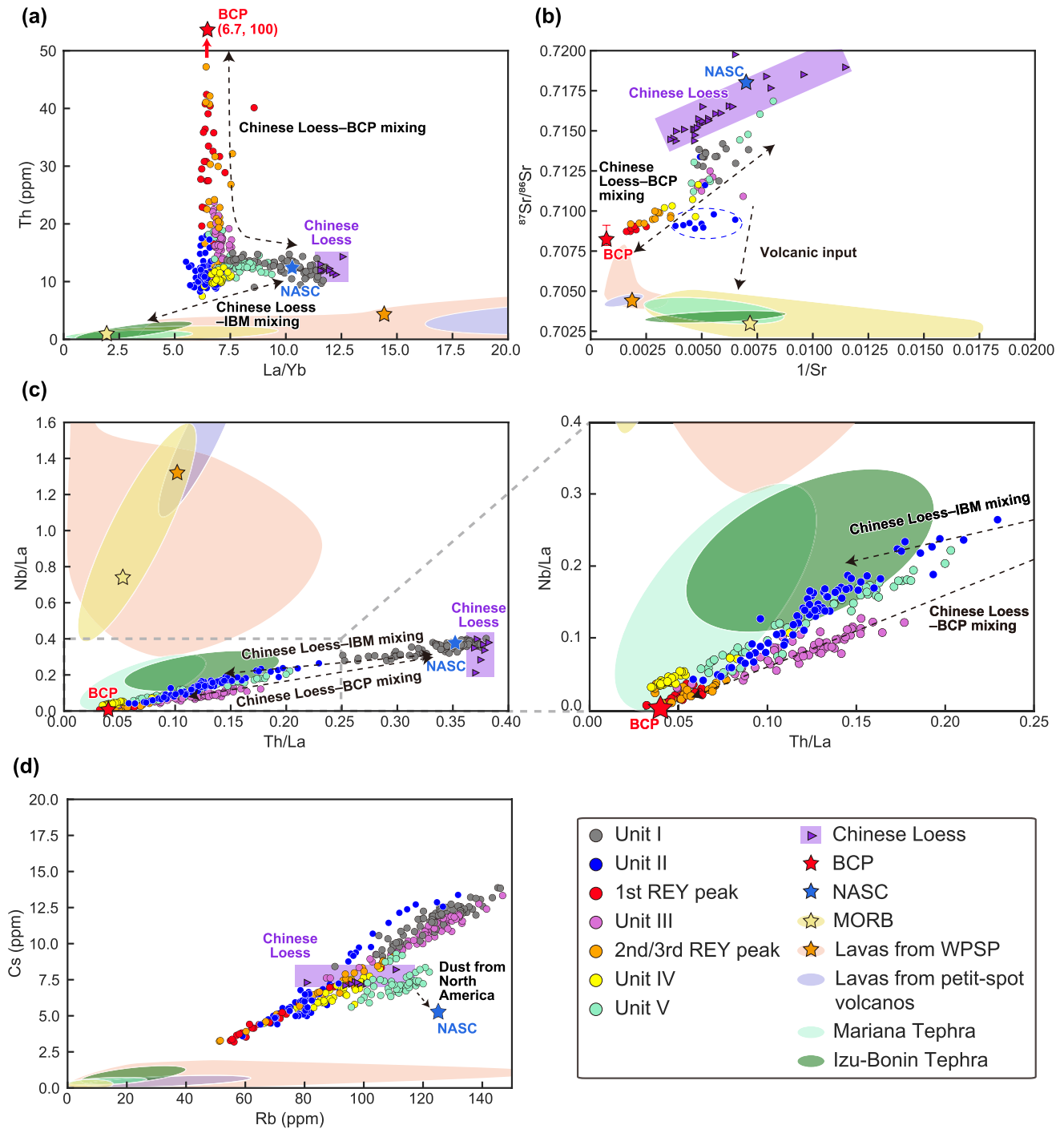


Figure 9.

Some of the Unit IV samples exhibit low Th and La/Yb values ($\text{Th} = \sim 10$ ppm, $\text{La}/\text{Yb} = \sim 7\text{--}7.5$) relative to those of Units I, III, V, and the REY peaks in Figure 9a, and exist near the Unit II samples in Figure 9b. These results suggest that the Unit IV samples may be affected by volcanic components, like Unit II. However, in Figure 9c, the Unit IV samples have lower Th/La values than those of Unit II. In addition, they show slightly higher Nb/La values compared to those of BCP and REY peaks and exist in the simple Chinese Loess-BCP mixing trend. Thus, the Unit IV values in Figures 9a–9c imply that the volcanic materials in Unit IV may be different from those in

Unit II, which has similar $1/\text{Sr}$ and $^{87}\text{Sr}/^{86}\text{Sr}$ values to those of the tephra from the IBM arc (Figure 9b), but higher La/Yb ratios than those of the tephra from the IBM arc (Figure 9a).

The Unit I samples on the scatter diagram between $1/\text{Sr}$ and $^{87}\text{Sr}/^{86}\text{Sr}$ show lower Sr isotope ratios than those of Chinese Loess, implying that Unit I could contain a certain amount of volcanic materials. Although it is not mentioned in previous studies, the shipboard core description recognized the presence of volcanic glass in the Unit I sediments in certain cases (e.g., MR13-E02 cores). Indeed, another two-component mixing model based on Sr isotope ratios suggested that the western North Pacific pelagic clay deposited during the last 3 Myr contains volcanic materials constituting up to 20%–25% (Asahara, 1999).

5.4. Implications for a Depositional History of the Western North Pacific Deep-Sea Sediments Since the Late Cretaceous

5.4.1. Change in the Sedimentary End-Members Around Minamitorishima Island

Our model calculation suggested a fundamental change in the sedimentary end-members around Minamitorishima Island during the depositional history of the area. As discussed above, the contributions of BCP and Mn oxides to the bulk chemical composition of the sediments are 0%–33% and 0%–5.5%, respectively (cf. Section 5.2, Table 1). These values are almost the same as the results based on microscopic observations reported by Ohta et al. (2016, 2020) and this study. According to the Sr-isotopic model calculations and bulk chemical compositions, the measured $^{87}\text{Sr}/^{86}\text{Sr}$ of the bulk sediments can be explained by the four-component model (terrigenous component, BCP, Mn oxides, and volcanic components) of the sediment column (cf. Section 5.3, Figures 7 and 9). The depth profiles of Sr isotope modeling illustrate almost the same trends as the analyzed Sr isotope ratios (Figure 7), which suggests (a) the effectiveness of the visual estimation by microscopic observations and (b) the validity of the assumption that eluted volcanic Sr has been almost maintained in the surrounding sediments. Significant volcanic inputs occurred at the following two intervals: from Unit II to the 1st REY peak and below the 2nd REY peak (i.e., Units IV and V), based on the smear slide observations. The maximum estimated contribution of the volcanic components is over 30% (Table S7 in Supporting Information S2). The bulk chemical compositions of Unit II and the 1st REY peak suggested that they could contain tephra from the IBM arc (cf. Section 5.3.3, Figure 9). This indicates that a substantial amount of volcanic material began to be supplied to the seafloor around Minamitorishima Island from the Izu-Bonin and Mariana arc during the deposition of Unit II and the 1st REY peak. The input of volcanic material from the Izu-Bonin and Mariana arc is consistent with the silicate fraction observed in the western North Pacific pelagic clay by Asahara (1999). In contrast, the bulk $^{87}\text{Sr}/^{86}\text{Sr}$ and chemical compositions revealed that the provenance of volcanic materials in Unit IV could be different from that of Unit II and the 1st REY peak (cf. Section 5.3.3, Figures 7 and 9), and those of Unit V are discussed in Section 5.4.3.

5.4.2. Relationship Between the Input of Volcanic Material and Geographical Setting

Here, the additional input of volcanic material to the study area is considered in terms of spatiotemporal changes in the geographical setting. The 1st REY peak and Unit II were deposited between the latest Eocene and the Eocene-Oligocene boundary, and between ~34 and ~15 Ma, respectively (Nozaki et al., 2019; Ohta et al., 2020;

Figure 9. Scatter diagrams of (a) La/Yb – Th , (b) $1/\text{Sr}$ – $^{87}\text{Sr}/^{86}\text{Sr}$, (c) Th/La – Nb/La with the enlarged view, and (d) Cs – Rb of bulk sediments collected from eight piston and six pilot cores: KR13-02 PC04, PC05, and PC06, MR13-E02 PC01 and PC03, MR14-E02 PC05 and PC08, MR15-E01 PC02, KR13-02 PCPL04, and MR14-E02 PCPL04, PCPL05, PCPL08, PCPL09, and PCPL11. The data of $^{87}\text{Sr}/^{86}\text{Sr}$ ratios are from this study and Yasukawa et al. (2019); the chemical composition data are from Fujinaga et al. (2016), Iijima et al. (2016), Takaya et al. (2018), Yasukawa et al. (2019), Tanaka, Nakamura, Yasukawa, Mimura, Fujinaga, Iijima et al. (2020), and this study. In the figures, the representative endmembers are also shown. Chinese Loess are from Taylor et al. (1983), Gallet et al. (1996), Jahn et al. (2001), Yokoo et al. (2004), and Chen et al. (2007); biogenic calcium phosphate (BCP) is from Takaya et al. (2018), and this study; North American Shale Composite is from Haskin et al. (1966), Gromet et al. (1984), and Pearce et al. (2015); MORB are from Class & Lehnert 2012; yellow area with the global average (yellow star; Gale et al., 2013; White & Klein, 2014); data on lavas from West Pacific Seamount Province are from the data set of Anawetak Seamount Trail, Gilbert Ridge Seamounts, Magellan Seamount Trail, Ratak Seamount Group, and Ujlan Seamounts retrieved from GeoROC, 2021a, 2021b, 2021c, 2021d, 2021e; orange area with the average value (orange star; Christie et al., 1995; Koppers et al., 2003); data on lavas from petit-spot volcanos are from Machida et al. (2009) and Miyazaki et al. (2015); tephra from the Mariana arc (40–23 Ma) is from Savov et al. (2006) and Straub et al. (2015, 2017); tephra from the Izu-Bonin arc (40–23 Ma) is from Bryant et al. (2003) and Straub et al. (2010). A blue dashed circle in (b) implies the Units I samples with low $^{87}\text{Sr}/^{86}\text{Sr}$ values, which are not located between the Unit I and the rare earth elements and yttrium (REY) peaks. As for (a) and (c), the mixing curves between Chinese Loess and BCP, and between Chinese Loess and the tephra from the Izu-Bonin arc with their reference ratios are shown in Figure S3 in Supporting Information S1.

Usui & Yamazaki, 2021). During these intervals, the input of volcanic materials from the Izu-Bonin-Mariana arc increased. Previous studies suggested that the mature IBM arc was formed in the late Eocene to early Oligocene (40–28 Ma) with explosive volcanism (37–28 Ma; Johnson et al., 2021; Shipboard Scientific Party, 2002). Therefore, the results of this study, as well as the estimated age of the volcanic activity of the IBM arc (i.e., the latest Eocene to Oligocene), suggest that the introduction of volcanic materials to the area around Minamitorishima Island could be caused by the explosive volcanism forming the mature IBM arc.

According to the paleogeographic reconstructions reported by Müller et al. (2019), Minamitorishima Island has remained in the east of the IBM arc at almost the same latitude since at least the middle Eocene (~45 Ma; Figure 10). Therefore, in addition to the regional tectonic activity, the northwestward movement of Minamitorishima Island toward the IBM arc due to Pacific Plate motion could also be responsible for the onset of volcanic input to the area around Minamitorishima Island. Although Hyeong et al. (2016) suggested that the ITCZ migrated across the equator from south to north during the global cooling around the Eocene-Oligocene boundary (~34.3–34.0 Ma), the Minamitorishima area was most likely under the influence of the westerlies around the Eocene-Oligocene transition, because of the increased input of the Mariana arc volcanic component to this area during the 1st REY peak and Unit II deposition. This implies that the volcanic materials from the IBM arc could be transported to the area located more than 3,000 km away at that time.

Unit IV could have also experienced an increase in volcanic components that could be different from those in Unit II (i.e., the tephra from the Izu-Bonin-Mariana arc), as discussed in Section 5.3.3. The depositional age of Unit IV has not been determined, but the onset of pelagic clay deposition around Minamitorishima Island was estimated to be ~75 Ma (Shipboard Scientific Party, 1990). Considering the paleo-location of the study area from 75 to ~34.4 Ma (Figure 10), the longitude of Minamitorishima Island was approximately 170°W–170°E in the central Pacific Ocean, which should have been several thousand kilometers from both the East Pacific Rise (EPR) and the IBM arc. This result implies that neither MORB from the EPR nor volcanic tephra from the IBM arc could have affected Unit IV. Therefore, further research on the volcanic activity that influenced Unit IV is necessary to explain the chemical compositional data (e.g., slightly high Nb/La in Figure 9c).

5.4.3. Change in Provenance of Terrigenous Component

The $^{87}\text{Sr}/^{86}\text{Sr}$ ratios of the four Unit V samples from MR15-E01 are the highest among all the samples (Figure 9b; Section 4.2). The higher Sr isotopic ratio may result from the difference in the terrigenous component. The $^{87}\text{Sr}/^{86}\text{Sr}$ ratio of the terrigenous component can reach 0.732 (Basile et al., 1997; Biscaye et al., 1997; Grousset & Biscaye, 2005; Kanayama et al., 2005; Pearce et al., 2015; Sun, 2005), which is clearly higher than the assumed values in this study ($^{87}\text{Sr}/^{86}\text{Sr} \approx 0.716$). Previous studies suggested that Asia and North/Central/South America may have served as source areas to provide eolian dust to the North Pacific (Hyong et al., 2011, 2016; Pettke et al., 2000, 2002; Stancin et al., 2006; Zhang et al., 2016), and the main dust source for the past 25 million years has been eastern Asia (Zhang et al., 2016). It is notable that dust from North America also has high Sr values ($^{87}\text{Sr}/^{86}\text{Sr} \approx 0.717\text{--}0.731$; Biscaye et al., 1997; McCulloch & Wasserburg, 1978; Pearce et al., 2015; Taylor et al., 1983), which are similar to those of the dust from Asia ($^{87}\text{Sr}/^{86}\text{Sr} \approx 0.714\text{--}0.734$; Chen et al., 2007; Gallet et al., 1996; Jahn et al., 2001; Kanayama et al., 2005; Sun, 2005; Yokoo et al., 2004).

The content values of Unit V are similar to those of Chinese Loess and Unit I; however, their La/Yb ratios are lower than those of Chinese Loess (Figure 9a). This tendency of Unit V is similar to that of the North American shale composite (NASC; Gromet et al., 1984; Haskin et al., 1966). In addition, in the scatter diagram between Rb and Cs (Figure 9d), the Unit V samples clearly deviate from the other units and REY peaks, shifting toward the NASC composition. These chemical compositional data support that North America could be considered the provenance of the terrigenous component in Unit V.

Focusing on the eastern Pacific Ocean, there was a substantial amount of volcanism in the Central/South America, such as the Caribbean Large Igneous province (CLIP; Hauff et al., 2000; Sinton et al., 1998) in the Late Cretaceous, and multiple explosive volcanic activities forming the ignimbrite and tephra layers in the Caribbean area during the Eocene and Miocene (Central American Tertiary Ignimbrite Province; Jordan et al., 2006, 2007). Although Unit V contains 1%–40% of phillipsite, which implies the input from substantial volcanic materials, the Caribbean volcanic activities do not account for the Sr isotope ratios or formation ages of the sediments: Unit V with higher Sr isotope ratios than the other units deposited between ~75 Ma and the latest Eocene,

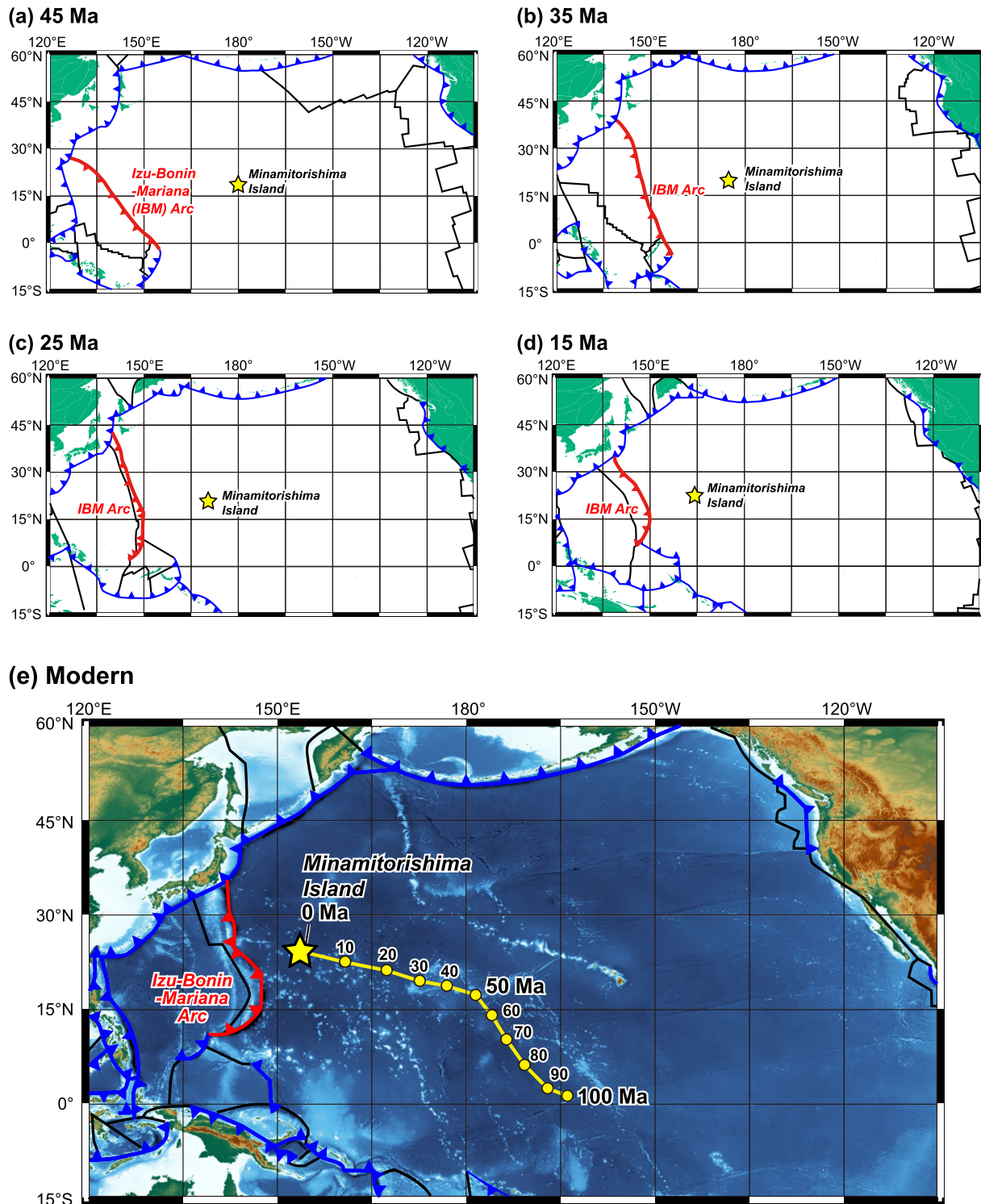


Figure 10. Reconstructed track of Minamitorishima Island with plate boundaries at (a) 45 Ma, (b) 35 Ma, (c) 25 Ma, (d) 15 Ma, and (e) modern. (a)–(d) Yellow star represents the paleoposition of Minamitorishima Island at each time slice. (e) Yellow circles represent paleopositions of Minamitorishima Island, plotted every 10 million years. Red lines with triangles indicate the Izu-Bonin-Mariana arc, blue lines with triangles indicate subduction zones, and solid black lines indicate mid-ocean ridges. Topography and bathymetry are based on ETOPO1 (NOAA National Geophysical Data Center, 2009; <https://www.ngdc.noaa.gov/mgg/global/global.html>). The reconstruction was created using GPlates software (<http://www.gplates.org>) and website (<http://portal.gplates.org/>); plate polygon and rotation data are from Müller et al. (2019).

whereas $^{87}\text{Sr}/^{86}\text{Sr} = 0.7030\text{--}0.7060$ at 92–74 Ma in CLIP, and $^{87}\text{Sr}/^{86}\text{Sr} = 0.7040\text{--}0.7069$ at 47–30 Ma and 24–12 Ma in the Central American Tertiary Ignimbrite Province (Hauff et al., 2000; Jordan et al., 2007; Sigurdsson et al., 2000). Although a part of the eruption age of the Central American Tertiary Ignimbrite Province is within the range of ~ 75 Ma to the latest Eocene, Carr et al. (2007) concluded that the prevailing wind direction around the province during the eruption was from west to east. Thus, it is unlikely that this volcanism was a source of materials for Unit V.

Meanwhile, the chemical and isotopic compositional features imply that the provenances of the terrigenous components of Units I and III may be different. The Unit III samples exhibit high Cs and Rb contents (Figures 8 and 9d) and are scattered on the mixing trend between Chinese Loess-BCP (Figure 9c), which implies that they are less affected by volcanic materials compared to the other units or REY peaks. On the other hand, the observed Rb content is higher than that calculated in Unit III (Figure 8) and may be attributed to a change in the terrigenous dust source. Indeed, the observed $^{87}\text{Sr}/^{86}\text{Sr}$ values of KR13-02 PC05 are lower than the calculated $^{87}\text{Sr}/^{86}\text{Sr}$ between 5.97 and 3.97 mbsf, Unit III, in all models (Figure 7). This tendency might be explained by a brief input of terrigenous components with low $^{87}\text{Sr}/^{86}\text{Sr}$ values. Based on the discussion on the dust source of Unit V mentioned above, it can be inferred that one possibility is a substantial input of Central/South American dust with low $^{87}\text{Sr}/^{86}\text{Sr}$ ratios, which could be eroded and transported by the trade winds, potentially affecting Unit III. Another possibility is the terrigenous components called “eolian 2,” which was deduced from ODP Site 1149 by Scudder et al. (2014), located east of the Izu-Bonin arc. They suggested the presence of a continental crustal material, other than the Chinese Loess, that had been supplied to the western North Pacific until the Paleogene when Unit III was deposited. In addition, the $^{87}\text{Sr}/^{86}\text{Sr}$ ratios of Chinese Loess used in this study were mainly obtained from the Pliocene section; therefore, the actual $^{87}\text{Sr}/^{86}\text{Sr}$ ratios of dust from Asia during the early Paleogene are unclear, and have the potential to lower the $^{87}\text{Sr}/^{86}\text{Sr}$ ratios of the deep-sea sediments. Therefore, based on the currently available data, we cannot constrain the provenance of Unit III. More comprehensive data for Unit III as well as Unit V, such as other isotope ratios (e.g., Nd, Pb, etc.), are required for future investigations.

6. Conclusions

This study measured the $^{87}\text{Sr}/^{86}\text{Sr}$ of deep-sea sediments, fish teeth (BCP), and Mn nodules collected from the seafloor around Minamitorishima Island in the western North Pacific Ocean. We demonstrated that the BCP could be affected by a diagenetic process, and thus its $^{87}\text{Sr}/^{86}\text{Sr}$ ratio seems to be different from that of seawater at the time of deposition. Mn oxides also show modern seawater-like $^{87}\text{Sr}/^{86}\text{Sr}$ values in all of the inner layers of the nodules, suggesting a continuous exchange of Sr between the Mn oxides and contemporary seawater.

According to the PAAS-normalized REY patterns, the sediment samples from the top of the cores (chemostratigraphic Unit I) are composed mainly of terrigenous materials, whereas the samples from the deeper part of the cores (chemostratigraphic Units II to V) are affected by the addition of other components with lower $^{87}\text{Sr}/^{86}\text{Sr}$ values compared to the continental crust, such as BCP and hydrogenous Mn oxides. The P_2O_5 content indicates that the proportion of BCP reached 12%–33% during the deposition of the 1st and 2nd REY peaks. In addition, the Co content suggests that the proportion of hydrogenous Mn oxides in Units II to V is 2%–5.5%.

Calculations of simple Sr mixing models and bulk chemical compositions of the samples revealed that four end-member components have been affected by the deep-sea sediments around Minamitorishima Island: a terrigenous component, BCP, hydrogenous Mn oxides, and a volcanic component. The input of volcanic materials increased in Unit II and the 1st REY peak, which originated from the Izu-Bonin-Mariana arc in the western North Pacific deposited since the latest Eocene explosive volcanism. In contrast, volcanic materials from a different source might have been introduced at Unit IV, although the depositional age and origin of the volcanic material are yet to be determined. We further recognized the differences in terrigenous components among Units I, III, and V. The provenance of the eolian dust could have shifted from North America in Unit V to eastern Asia in Unit I through the depositional history around the Minamitorishima area, although that in Unit III is unknown.

Conflict of Interest

The authors declare no conflicts of interest relevant to this study.

Data Availability Statement

The data used in this study were stored in the EarthChem database (DOI: <https://doi.org/10.26022/IEDA/112201>, and <https://doi.org/10.26022/IEDA/112200>).

Acknowledgments

The authors thank the shipboard scientific parties and crews of R/Vs Kairei, Mirai, and Yokosuka, and the operating team of SHINKAI 6500 for their dedicated work. The authors are grateful to R. Usami, K. Horinouchi, W. Zhang, H. Higuchi, M. Kanazawa, Y. Itabashi, and C. Kabashima for their assistance with the chemical analyses. This research was financially supported by the Japan Society for the Promotion of Science (JSPS) KAKENHI Grants (No. JP15H05771 to Y.K., No. JP25289334 and No. JP17H01361 to N.K., No. JP18K14168 and No. JP20H02678 to K.Y., and No. JP18J22633 and No. JP21J00998 to E.T.). This study was supported by the Council for Science, Technology and Innovation (CSTI) and the Cross-ministerial Strategic Innovation Promotion Program (SIP) "Next-generation technology for ocean resources exploration."

References

- Amakawa, H., Usui, A., Iijima, K., & Suzuki, K. (2017). Surface layer Nd isotopic composition of ferromanganese crusts collected from the Takuyo-Daigo Seamount reflects ambient seawater. *Geochemical Journal*, *51*(1), e1–e7. <https://doi.org/10.2343/geochemj.2.0463>
- Arculus, R. J., Ishizuka, O., Bogus, K. A., Gurnis, M., Hickey-Vargas, R., Aljehdali, M. H., et al. (2015). A record of spontaneous subduction initiation in the Izu-Bonin-Mariana arc. *Nature Geoscience*, *8*(9), 728–733. <https://doi.org/10.1038/ngeo2515>
- Arrhenius, G., Bramlette, M. N., & Picciotto, E. (1957). Localization of radioactive and stable heavy nuclides in ocean sediments. *Nature*, *180*(4576), 85–86. <https://doi.org/10.1038/180085a0>
- Asahara, Y. (1999). ⁸⁷Sr/⁸⁶Sr variation in North Pacific sediments: A record of the Milankovitch cycle in the past 3 million years. *Earth and Planetary Science Letters*, *171*(3), 453–464. [https://doi.org/10.1016/S0012-821X\(99\)00158-2](https://doi.org/10.1016/S0012-821X(99)00158-2)
- Asahara, Y., Tanaka, T., Kamioka, H., & Nishimura, A. (1995). Asian continental nature of ⁸⁷Sr/⁸⁶Sr ratios in north central Pacific sediments. *Earth and Planetary Science Letters*, *133*(1–2), 105–116. [https://doi.org/10.1016/0012-821X\(95\)00048-H](https://doi.org/10.1016/0012-821X(95)00048-H)
- Asahara, Y., Tanaka, T., Kamioka, H., Nishimura, A., & Yamazaki, T. (1999). Provenance of the north Pacific sediments and process of source material transport as derived from Rb–Sr isotopic systematics. *Chemical Geology*, *158*(3–4), 271–291. [https://doi.org/10.1016/S0009-2541\(99\)00056-X](https://doi.org/10.1016/S0009-2541(99)00056-X)
- Azami, K., Hirano, N., Machida, S., Yasukawa, K., & Kato, Y. (2018). Rare earth elements and yttrium (REY) variability with water depth in hydrogenetic ferromanganese crusts. *Chemical Geology*, *493*, 224–233. <https://doi.org/10.1016/j.chemgeo.2018.05.045>
- Basile, I., Grousset, F. E., Revel, M., Petit, J. R., Biscaye, P. E., & Barkov, N. I. (1997). Patagonian origin of glacial dust deposited in East Antarctica (Vostok and Dome C) during glacial stages 2, 4, and 6. *Earth and Planetary Science Letters*, *146*(3–4), 573–589. [https://doi.org/10.1016/S0012-821X\(96\)00255-5](https://doi.org/10.1016/S0012-821X(96)00255-5)
- Bernat, M. (1975). Les isotopes de l'uranium et du thorium et les terres rares dans l'environnement marin. *Cahiers ORSTOM-Serie Geologie*, *7*, 65–83.
- Bernat, M., Bieri, R. H., Koide, M., Griffin, J. J., & Goldberg, E. D. (1970). Uranium, thorium, potassium, and argon in marine phillipsites. *Geochimica et Cosmochimica Acta*, *34*(10), 1053–1071. [https://doi.org/10.1016/0016-7037\(70\)90162-6](https://doi.org/10.1016/0016-7037(70)90162-6)
- Bernat, M., & Goldberg, E. D. (1968). Thorium isotopes in the marine environment. *Earth and Planetary Science Letters*, *5*, 308–312. [https://doi.org/10.1016/S0012-821X\(68\)80057-3](https://doi.org/10.1016/S0012-821X(68)80057-3)
- Biscaye, P. E., Grousset, F. E., Revel, M., Van Der Gaast, S., Zielinski, G. A., Vaars, A., & Kukla, G. (1997). Asian provenance of glacial dust (stage 2) in the Greenland Ice Sheet Project 2 Ice Core, Summit, Greenland. *Journal of Geophysical Research*, *102*(C12), 26765–26781. <https://doi.org/10.1029/97JC01249>
- Brandl, P. A., Hamada, M., Arculus, R. J., Johnson, K., Marsaglia, K. M., Savov, I. P., et al. (2017). The arc arises: The links between volcanic output, arc evolution and melt composition. *Earth and Planetary Science Letters*, *461*, 73–84. <https://doi.org/10.1016/j.epsl.2016.12.027>
- Broecker, W. S., & Peng, T. H. (1982). *Tracers in the sea*. Columbia University. <https://doi.org/10.1017/S003382220000522>
- Brounce, M., Reagan, M. K., Kelley, K. A., Cottrell, E., Shimizu, K., & Almeev, R. (2021). Covariation of slab tracers, volatiles, and oxidation during subduction initiation. *Geochemistry, Geophysics, Geosystems*, *22*(6), e2021GC009823. <https://doi.org/10.1029/2021GC009823>
- Bryant, C. J., Arculus, R. J., & Eggins, S. M. (2003). The geochemical evolution of the Izu-Bonin arc system: A perspective from tephra recovered by Deep-sea drilling. *Geochemistry, Geophysics, Geosystems*, *4*(11), 1094. <https://doi.org/10.1029/2002GC000427>
- Capo, R. C., Stewart, B. W., & Chadwick, O. A. (1998). Strontium isotopes as tracers of ecosystem processes: Theory and methods. *Geoderma*, *82*, 197–225. [https://doi.org/10.1016/S0016-7061\(97\)00102-x](https://doi.org/10.1016/S0016-7061(97)00102-x)
- Carr, M., Patino, L., & Feigenson, M. (2007). Petrology and geochemistry of lavas. In J. Bundschuh, & G. E. Alvarado (Eds.), *Central America: Geology, resources and hazards* (pp. 565–577). Taylor & Francis. <https://doi.org/10.1201/9780203947043.ch22>
- Chen, J., Li, G., Yang, J., Rao, W., Lu, H., Balsam, W., et al. (2007). Nd and Sr isotopic characteristics of Chinese deserts: Implications for the provenances of Asian dust. *Geochimica et Cosmochimica Acta*, *71*(15), 3904–3914. <https://doi.org/10.1016/j.gca.2007.04.033>
- Christie, D. M., Dieu, J. J., & Gee, J. S. (1995). Petrologic studies of basement lavas from northwest Pacific guyots. In J. A. Haggerty, I. Premoli Silva, F. Rack, & M. K. McNutt (Eds.), *Proceedings of the ocean drilling program, 144 scientific results* (Vol. 144, pp. 495–512). Ocean Drilling Program. <https://doi.org/10.2973/odp.proc.sr.144.028.1995>
- Class, C., & Lehnert, K. (2012). *PetDB Expert MORB (Mid-Ocean Ridge Basalt) Compilation*. <https://doi.org/10.1594/IEDA/100060>
- Clauer, N., Stille, P., Bonnot-Courtois, C., & Moore, W. S. (1984). Nd–Sr isotopic and REE constraints on the genesis of hydrothermal manganese crusts in the Galapagos. *Nature*, *311*(5988), 743–745. <https://doi.org/10.1038/311743a0>
- Czyscinski, K. (1973). Authigenic phillipsite formation rates in the central Indian Ocean and the equatorial Pacific Ocean. *Deep-Sea Research and Oceanographic Abstracts*, *20*(6), 555–559. [https://doi.org/10.1016/0011-7471\(73\)90079-X](https://doi.org/10.1016/0011-7471(73)90079-X)
- Dubinin, A. V., Uspenskaya, T. Y., Rimszkaya-Korsakova, M. N., & Demidova, T. P. (2017). Rare elements and Nd and Sr isotopic composition in micronodules from the Brazil Basin, Atlantic Ocean. *Lithology and Mineral Resources*, *52*(2), 81–101. <https://doi.org/10.1134/S0024490217020043>
- Dunlea, A. G., Murray, R. W., Sauvage, J., Pockalny, R. A., Spivack, A. J., Harris, R. N., & D'Hondt, S. (2015). Cobalt-based age models of pelagic clay in the South Pacific Gyre. *Geochemistry, Geophysics, Geosystems*, *16*(8), 2694–2710. <https://doi.org/10.1002/2015GC005892>
- Dunlea, A. G., Murray, R. W., Sauvage, J., Spivack, A. J., Harris, R. N., & D'Hondt, S. (2015). Dust, volcanic ash, and the evolution of the south Pacific gyre through the Cenozoic. *Paleoceanography*, *30*(8), 1078–1099. <https://doi.org/10.1002/2015PA002829>
- Frank, M. (2002). Radiogenic isotopes: Tracers of past ocean circulation and erosional input. *Reviews of Geophysics*, *40*(1), 1–38. <https://doi.org/10.1029/2000RG000094>
- Fujinaga, K., Yasukawa, K., Nakamura, K., Machida, S., Takaya, Y., Ohta, J., et al. (2016). Geochemistry of REY-rich mud in the Japanese exclusive economic zone around Minamitorishima island. *Geochemical Journal*, *50*(6), 575–590. <https://doi.org/10.2343/geochemj.2.0432>
- Gale, A., Dalton, C. A., Langmuir, C. H., Su, Y., & Schilling, J.-G. (2013). The mean composition of ocean ridge basalts. *Geochemistry, Geophysics, Geosystems*, *14*(3), 489–518. <https://doi.org/10.1029/2012GC004334>
- Gallet, S., Jahn, B., & Torii, M. (1996). Geochemical characterization of the Luochuan loess-paleosol sequence, China, and paleoclimatic implications. *Chemical Geology*, *133*(1–4), 67–88. [https://doi.org/10.1016/S0009-2541\(96\)00070-8](https://doi.org/10.1016/S0009-2541(96)00070-8)

- GeoROC (2021a). *Anewetak seamount trail*. Retrieved from http://georoc.mpch-mainz.gwdg.de/georoc/Csv_Downloads/Seamounts_comp/s_ANEWETAK_SEAMOUNT_TRAIL.csv
- GeoROC (2021b). *Gilbert Ridge Seamounts*. Retrieved from http://georoc.mpch-mainz.gwdg.de/georoc/Csv_Downloads/Seamounts_comp/s_GILBERT_RIDGE_SEAMOUNTS.csv
- GeoROC (2021c). *Magellan seamount trail*. Retrieved from http://georoc.mpch-mainz.gwdg.de/georoc/Csv_Downloads/Seamounts_comp/s_MAGELLAN_SEAMOUNT_TRAIL.csv
- GeoROC (2021d). *Ratak seamount group*. Retrieved from http://georoc.mpch-mainz.gwdg.de/georoc/Csv_Downloads/Seamounts_comp/s_RATAK_SEAMOUNT_GROUP.csv
- GeoROC (2021e). *Ujlan seamounts*. Retrieved from http://georoc.mpch-mainz.gwdg.de/georoc/Csv_Downloads/Seamounts_comp/s_UJLAN_SEAMOUNTS.csv
- Gleason, J. D., Moore, T. C., Rea, D. K., Johnson, T. M., Owen, R. M., Blum, J. D., et al. (2002). Ichthyolith strontium isotope stratigraphy of a neogene red clay sequence: Calibrating eolian dust accumulation rates in the central North Pacific. *Earth and Planetary Science Letters*, 202(3–4), 625–636. [https://doi.org/10.1016/S0012-821X\(02\)00827-0](https://doi.org/10.1016/S0012-821X(02)00827-0)
- Godfrey, L. V. (2002). Temporal changes in the lead isotopic composition of red clays: Comparison with ferromanganese crust records. *Chemical Geology*, 185(3–4), 241–254. [https://doi.org/10.1016/S0009-2541\(01\)00406-5](https://doi.org/10.1016/S0009-2541(01)00406-5)
- Gromet, L. P., Haskin, L. A., Korotev, R. L., & Dymek, R. F. (1984). The “North American shale composite”: Its compilation, major and trace element characteristics. *Geochimica et Cosmochimica Acta*, 48(12), 2469–2482. [https://doi.org/10.1016/0016-7037\(84\)90298-9](https://doi.org/10.1016/0016-7037(84)90298-9)
- Grousset, F. E., & Biscaye, P. E. (2005). Tracing dust sources and transport patterns using Sr, Nd and Pb isotopes. *Chemical Geology*, 222(3–4), 149–167. <https://doi.org/10.1016/j.chemgeo.2005.05.006>
- Halbach, P., & Puteanus, D. (1984). The influence of the carbonate dissolution rate on the growth and composition of Co-rich ferromanganese crusts from Central Pacific seamount areas. *Earth and Planetary Science Letters*, 68(1), 73–87. [https://doi.org/10.1016/0012-821X\(84\)90141-9](https://doi.org/10.1016/0012-821X(84)90141-9)
- Hall, R. (2002). Cenozoic geological and plate tectonic evolution of SE Asia and the SW Pacific: Computer-based reconstructions, model and animations. *Journal of Asian Earth Sciences*, 20(4), 353–431. [https://doi.org/10.1016/S1367-9120\(01\)00069-4](https://doi.org/10.1016/S1367-9120(01)00069-4)
- Haskin, L. A., Wildeman, T. R., Frey, F. A., Collins, K. A., Keedy, C. R., & Haskin, M. A. (1966). Rare earths in sediments. *Journal of Geophysical Research*, 71(24), 6091–6105. <https://doi.org/10.1029/JZ071i024p06091>
- Hauff, F., Hoernle, K., Tilton, G., Graham, D. W., & Kerr, A. C. (2000). Large volume recycling of oceanic lithosphere over short time scales: Geochemical constraints from the Caribbean Large Igneous Province. *Earth and Planetary Science Letters*, 174(3–4), 247–263. [https://doi.org/10.1016/S0012-821X\(99\)00272-1](https://doi.org/10.1016/S0012-821X(99)00272-1)
- Hein, J. R., & Koschinsky, A. (2014). Deep-ocean ferromanganese crusts and nodules. In H. D. Holland, & K. K. Turekian (Eds.), *Treatise on Geochemistry* (Vol. 13, pp. 273–291). Elsevier. <https://doi.org/10.1016/B978-0-08-095975-7.01111-6>
- Hirano, N. (2011). Petit-spot volcanism: A new type of volcanic zone discovered near a trench. *Geochemical Journal*, 45(2), 157–167. <https://doi.org/10.2343/geochemj.1.0111>
- Hirano, N., Koppers, A. A. P., Takahashi, A., Fujiwara, T., & Nakanishi, M. (2008). Seamounts, knolls and petit-spot monogenetic volcanoes on the subducting Pacific plate. *Basin Research*, 20(4), 543–553. <https://doi.org/10.1111/j.1365-2117.2008.00363.x>
- Hirano, N., Machida, S., Sumino, H., Shimizu, K., Tamura, A., Morishita, T., et al. (2019). Petit-spot volcanoes on the oldest portion of the Pacific plate. *Deep Sea Research Part I: Oceanographic Research Papers*, 154, 103142. <https://doi.org/10.1016/j.dsr.2019.103142>
- Holland, H. D. (1984). *The chemical evolution of the atmosphere and oceans*. Princeton University Press.
- Hyeong, K., Kim, J., Pettke, T., Yoo, C. M., & Hur, S. Do. (2011). Lead, Nd and Sr isotope records of pelagic dust: Source indication versus the effects of dust extraction procedures and authigenic mineral growth. *Chemical Geology*, 286(3–4), 240–251. <https://doi.org/10.1016/j.chemgeo.2011.05.009>
- Hyeong, K., Kuroda, J., Seo, I., & Wilson, P. A. (2016). Response of the Pacific inter-tropical convergence zone to global cooling and initiation of Antarctic glaciation across the Eocene Oligocene Transition. *Scientific Reports*, 6, 30647. <https://doi.org/10.1038/srep30647>
- Iijima, K., Yasukawa, K., Fujinaga, K., Nakamura, K., Machida, S., Takaya, Y., et al. (2016). Discovery of extremely REY-rich mud in the western North Pacific Ocean. *Geochemical Journal*, 50(6), 557–573. <https://doi.org/10.2343/geochemj.2.0431>
- Ingram, B. L. (1995). Ichthyolith strontium isotopic stratigraphy of deep-sea clays: Sites 885 and 886 (North Pacific Transect). In D. K. Rea, I. A. Basov, D. W. Scholl, & J. F. Allan (Eds.), *Proceedings of the ocean drilling program, 145 scientific results* (Vol. 145, pp. 399–412). Ocean Drilling Program. <https://doi.org/10.2973/odp.proc.sr.145.130.1995>
- Ishizuka, O., Hickey-Vargas, R., Arculus, R. J., Yogodzinski, G. M., Savov, I. P., Kusano, Y., et al. (2018). Age of Izu–Bonin–Mariana arc base-ment. *Earth and Planetary Science Letters*, 481, 80–90. <https://doi.org/10.1016/j.epsl.2017.10.023>
- Ishizuka, O., Tani, K., Reagan, M. K., Kanayama, K., Umino, S., Harigane, Y., et al. (2011). The timescales of subduction initiation and subsequent evolution of an oceanic island arc. *Earth and Planetary Science Letters*, 306(3–4), 229–240. <https://doi.org/10.1016/j.epsl.2011.04.006>
- Ishizuka, O., Taylor, R. N., Yuasa, M., & Ohara, Y. (2011). Making and breaking an island arc: A new perspective from the Oligocene Kyushu–Palau arc, Philippine Sea. *Geochemistry, Geophysics, Geosystems*, 12(5), Q05005. <https://doi.org/10.1029/2010GC003440>
- Ito, T., Usui, A., Kajiwar, Y., & Nakano, T. (1998). Strontium isotopic compositions and paleoceanographic implication of fossil manganese nodules in DSDP/ODP cores, Leg 1–126. *Geochimica et Cosmochimica Acta*, 62(9), 1545–1554. [https://doi.org/10.1016/S0016-7037\(98\)00051-9](https://doi.org/10.1016/S0016-7037(98)00051-9)
- Jahn, B. M., Gallet, S., & Han, J. (2001). Geochemistry of the Xining, Xifeng and Jixian sections, Loess Plateau of China: Eolian dust provenance and paleosol evolution during the last 140 ka. *Chemical Geology*, 178(1–4), 71–94. [https://doi.org/10.1016/S0009-2541\(00\)00430-7](https://doi.org/10.1016/S0009-2541(00)00430-7)
- Johnson, K., Marsaglia, K. M., Brandl, P. A., Barth, A. P., Waldman, R., Ishizuka, O., et al. (2021). Intra-oceanic submarine arc evolution recorded in an ~1-km-thick rear-arc succession of distal volcanoclastic lobe deposits. *Geosphere*, 17(4), 957–980. <https://doi.org/10.1130/GES02321.1>
- Jones, C. E., Halliday, A. N., Rea, D. K., & Owen, R. M. (1994). Neodymium isotopic variations in North Pacific modern silicate sediment and the insignificance of detrital REE contributions to seawater. *Earth and Planetary Science Letters*, 127(1–4), 55–66. [https://doi.org/10.1016/0012-821X\(94\)90197-X](https://doi.org/10.1016/0012-821X(94)90197-X)
- Jones, C. E., Halliday, A. N., Rea, D. K., & Owen, R. M. (2000). Eolian inputs of lead to the North Pacific. *Geochimica et Cosmochimica Acta*, 64(8), 1405–1416. [https://doi.org/10.1016/S0016-7037\(99\)00439-1](https://doi.org/10.1016/S0016-7037(99)00439-1)
- Jordan, B. R., Sigurdsson, H., Carey, S., Lundin, S., Rogers, R. D., Singer, B., & Barquero-Molina, M. (2007). *Petrogenesis of Central American Tertiary Ignimbrites and Associated Caribbean Sea Tephra* (Vol. 428, pp. 151–179). Special Paper of the Geological Society of America. <https://doi.org/10.1130/2007.242807>
- Jordan, B. R., Sigurdsson, H., Carey, S. N., Rogers, R., & Ehrenborg, J. (2006). *Geochemical correlation of Caribbean Sea tephra layers with ignimbrites in Central America* (Vol. 402, pp. 175–208). Special Paper of the Geological Society of America. <https://doi.org/10.1130/2006.240208>
- Kanayama, S., Yabuki, S., Zeng, F., Liu, M., Shen, Z., Liu, L., et al. (2005). Size-dependent geochemical characteristics of Asian dust–Sr and Nd isotope compositions as tracers for source identification. *Journal of the Meteorological Society of Japan*, 83(3), 107–120. <https://doi.org/10.2151/jmsj.83A.107>

- Kashiwabara, T., Toda, R., Fujinaga, K., Honma, T., Takahashi, Y., & Kato, Y. (2014). Determination of host phase of Lanthanum in deep-sea REY-rich mud by XAFS and μ -XRF Using high-energy synchrotron radiation. *Chemistry Letters*, 43(2), 199–200. <https://doi.org/10.1246/cl.130853>
- Kashiwabara, T., Toda, R., Nakamura, K., Yasukawa, K., Fujinaga, K., Kubo, S., et al. (2018). Synchrotron X-ray spectroscopic perspective on the formation mechanism of REY-rich muds in the Pacific Ocean. *Geochimica et Cosmochimica Acta*, 240, 274–292. <https://doi.org/10.1016/j.gca.2018.08.013>
- Kato, Y., Fujinaga, K., Nakamura, K., Takaya, Y., Kitamura, K., Ohta, J., et al. (2011). Deep-sea mud in the Pacific Ocean as a potential resource for rare-earth elements. *Nature Geoscience*, 4(8), 535–539. <https://doi.org/10.1038/ngeo1185>
- Kato, Y., Fujinaga, K., & Suzuki, K. (2005). Major and trace element geochemistry and Os isotopic composition of metalliferous umbers from the Late Cretaceous Japanese accretionary complex. *Geochemistry, Geophysics, Geosystems*, 6(7), Q07004. <https://doi.org/10.1029/2005GC000920>
- Kato, Y., Nakao, K., & Isozaki, Y. (2002). Geochemistry of late permian to early triassic pelagic cherts from southwest Japan: Implications for an oceanic redox change. *Chemical Geology*, 182(1), 15–34. [https://doi.org/10.1016/S0009-2541\(01\)00273-X](https://doi.org/10.1016/S0009-2541(01)00273-X)
- Kato, Y., Ohta, I., Tsunematsu, T., Watanabe, Y., Isozaki, Y., Maruyama, S., & Imai, N. (1998). Rare earth element variations in mid-Archean banded iron formations: Implications for the chemistry of ocean and continent and plate tectonics. *Geochimica et Cosmochimica Acta*, 62(21–22), 3475–3497. [https://doi.org/10.1016/S0016-7037\(98\)00253-1](https://doi.org/10.1016/S0016-7037(98)00253-1)
- Koppers, A. A. P., Staudigel, H., Pringle, M. S., & Wijbrans, J. R. (2003). Short-lived and discontinuous intraplate volcanism in the South Pacific: Hot spots or extensional volcanism? *Geochemistry, Geophysics, Geosystems*, 4(10), 1089. <https://doi.org/10.1029/2003GC000533>
- Kutterolf, S., Schindlbeck, J. C., Robertson, A. H. F., Avery, A., Baxter, A. T., Petronotis, K., & Wang, K. L. (2018). Tephrostratigraphy and provenance from IODP Expedition 352, Izu-Bonin arc: Tracing tephra sources and volumes from the Oligocene to recent. *Geochemistry, Geophysics, Geosystems*, 19(1), 150–174. <https://doi.org/10.1002/2017GC007100>
- Kyte, F. T., Leinen, M., Ross Heath, G., & Zhou, L. (1993). Cenozoic sedimentation history of the central North Pacific: Inferences from the elemental geochemistry of core LL44-GPC3. *Geochimica et Cosmochimica Acta*, 57, 1719–1740. [https://doi.org/10.1016/0016-7037\(93\)90109-A](https://doi.org/10.1016/0016-7037(93)90109-A)
- Langmuir, C. H., Vocke, R. D., Hanson, G. N., & Hart, S. R. (1978). A general mixing equation with applications to Icelandic basalts. *Earth and Planetary Science Letters*, 37(3), 380–392. [https://doi.org/10.1016/0012-821X\(78\)90053-5](https://doi.org/10.1016/0012-821X(78)90053-5)
- Ling, H. F., Jiang, S. Y., Frank, M., Zhou, H. Y., Zhou, F., Lu, Z. L., et al. (2005). Differing controls over the Cenozoic Pb and Nd isotope evolution of deepwater in the central North Pacific Ocean. *Earth and Planetary Science Letters*, 232(3–4), 345–361. <https://doi.org/10.1016/j.epsl.2004.12.009>
- Machida, S., Fujinaga, K., Ishii, T., Nakamura, K., Hirano, N., & Kato, Y. (2016). Geology and geochemistry of ferromanganese nodules in the Japanese exclusive economic zone around Minamitorishima Island. *Geochemical Journal*, 50(6), 539–555. <https://doi.org/10.2343/geochemj.2.0419>
- Machida, S., Hirano, N., & Kimura, J. (2009). Evidence for recycled plate material in Pacific upper mantle unrelated to plumes. *Geochimica et Cosmochimica Acta*, 73(10), 3028–3037. <https://doi.org/10.1016/j.gca.2009.01.026>
- Machida, S., Nakamura, K., Kogiso, T., Shimomura, R., Horinouchi, K., Okino, K., & Kato, Y. (2021). Fine-scale chemostratigraphy of cross-sectioned hydrogenous ferromanganese nodules from the western North Pacific. *Island Arc*, 30(1), e12395. <https://doi.org/10.1111/iar.12395>
- Machida, S., Sato, T., Yasukawa, K., Nakamura, K., Iijima, K., Nozaki, T., & Kato, Y. (2021). Visualisation method for the broad distribution of seafloor ferromanganese deposits. *Marine Georesources & Geotechnology*, 39(3), 267–279. <https://doi.org/10.1080/1064119X.2019.1696432>
- Martin, E. E., & Scher, H. D. (2004). Preservation of seawater Sr and Nd isotopes in fossil fish teeth: Bad news and good news. *Earth and Planetary Science Letters*, 220(1–2), 25–39. [https://doi.org/10.1016/S0012-821X\(04\)00030-5](https://doi.org/10.1016/S0012-821X(04)00030-5)
- Mazzullo, J., & Graham, A. G. (1988). *Handbook for shipboard sedimentologists*. Ocean Drilling Program. <https://doi.org/10.2973/odp.tn.8.1988>
- McArthur, J. M., Howarth, R. J., & Shields, G. A. (2012). Strontium isotope stratigraphy. In F. Goldstein, J. Ogg, M. Schmitz, & G. Ogg (Eds.), *The geologic time scale 2012* (pp. 127–144). Elsevier. <https://doi.org/10.1016/B978-0-444-59425-9.00007-X>
- McArthur, J. M., Howarth, R. J., Shields, G. A., & Zhou, Y. (2020). Strontium isotope stratigraphy. In F. Goldstein, J. Ogg, M. Schmitz, & G. Ogg (Eds.), *Geologic time scale 2020* (pp. 211–238). Elsevier. <https://doi.org/10.1016/B978-0-12-824360-2.00007-3>
- McCulloch, M. T., & Wasserburg, G. J. (1978). Sm-Nd and Rb-Sr chronology of continental crust formation. *Science*, 200(4345), 1003–1011. <https://doi.org/10.1126/science.200.4345.1003>
- Mimura, K., Nakamura, K., Yasukawa, K., Machida, S., Ohta, J., Fujinaga, K., & Kato, Y. (2019). Significant impacts of pelagic clay on average chemical composition of subducting sediments: New insights from discovery of extremely rare-earth elements and yttrium-rich mud at Ocean Drilling Program Site 1149 in the western North Pacific Ocean. *Journal of Asian Earth Sciences*, 186, 104059. <https://doi.org/10.1016/j.jseas.2019.104059>
- Miyazaki, T., Hanyu, T., Kimura, J. I., Senda, R., Vaglarov, B. S., Chang, Q., et al. (2018). Clinopyroxene and bulk rock Sr–Nd–Hf–Pb isotope compositions of Raivavae ocean island basalts: Does clinopyroxene record early stage magma chamber processes? *Chemical Geology*, 482, 18–31. <https://doi.org/10.1016/j.chemgeo.2017.12.015>
- Miyazaki, T., Kimura, J. I., & Katakuse, M. (2016). Geochemical records from loess deposits in Japan over the last 210 kyr: Lithogenic source changes and paleoclimatic indications. *Geochemistry, Geophysics, Geosystems*, 17(7), 2745–2761. <https://doi.org/10.1002/2016GC006322>
- Miyazaki, T., Kimura, J. I., Senda, R., Vaglarov, B. S., Chang, Q., Takahashi, T., et al. (2015). Missing western half of the Pacific Plate: Geochemical nature of the Izanagi-Pacific Ridge interaction with a stationary boundary between the Indian and Pacific mantles. *Geochemistry, Geophysics, Geosystems*, 16(9), 3309–3332. <https://doi.org/10.1002/2015GC005911>
- Miyazaki, T., Vaglarov, B. S., Takei, M., Suzuki, M., Suzuki, H., Ohsawa, K., et al. (2012). Development of a fully automated open-column chemical separation system-COLUMN SPIDER-and its application to Sr-Nd-Pb isotope analyses of igneous rock samples. *Journal of Mineralogical and Petrological Sciences*, 107(2), 74–86. <https://doi.org/10.2465/jmps.110520>
- Müller, R. D., Zahirovic, S., Williams, S. E., Cannon, J., Seton, M., Bower, D. J., et al. (2019). A global plate model including lithospheric deformation along major rifts and orogens since the triassic. *Tectonics*, 38(6), 1884–1907. <https://doi.org/10.1029/2018TC005462>
- Nakai, S., Halliday, A. N., & Rea, D. K. (1993). Provenance of dust in the Pacific Ocean. *Earth and Planetary Science Letters*, 119(1–2), 143–157. [https://doi.org/10.1016/0012-821X\(93\)90012-X](https://doi.org/10.1016/0012-821X(93)90012-X)
- NOAA National Geophysical Data Center. (2009). *ETOPO1 1 Arc-minute global relief model*. NOAA National Centers for Environmental Information. <https://doi.org/10.7289/V5C8276M>
- Nozaki, T., Ohta, J., Noguchi, T., Sato, H., Ishikawa, A., Takaya, Y., et al. (2019). A Miocene impact ejecta layer in the pelagic Pacific Ocean. *Scientific Reports*, 9(1), 16111. <https://doi.org/10.1038/s41598-019-52709-1>
- Ohta, A., & Kawabe, I. (2001). REE(III) adsorption onto Mn dioxide (δ -MnO₂) and Fe oxyhydroxide: Ce(III) oxidation by δ -MnO₂. *Geochimica et Cosmochimica Acta*, 65(5), 695–703. [https://doi.org/10.1016/S0016-7037\(00\)00578-0](https://doi.org/10.1016/S0016-7037(00)00578-0)

- Ohta, J., Yasukawa, K., Machida, S., Fujinaga, K., Nakamura, K., Takaya, Y., et al. (2016). Geological factors responsible for REY-rich mud in the western North Pacific Ocean: Implications from mineralogy and grain size distributions. *Geochemical Journal*, *50*(6), 591–603. <https://doi.org/10.2343/geochemj.2.0435>
- Ohta, J., Yasukawa, K., Nozaki, T., Takaya, Y., Mimura, K., Fujinaga, K., et al. (2020). Fish proliferation and rare-earth deposition by topographically induced upwelling at the late Eocene cooling event. *Scientific Reports*, *10*(1), 9896. <https://doi.org/10.1038/s41598-020-66835-8>
- Pälike, H., Lyle, M. W., Nishi, H., Raffi, I., Ridgwell, A., Gamage, K., et al. (2012). A Cenozoic record of the equatorial Pacific carbonate compensation depth. *Nature*, *488*, 609–614. <https://doi.org/10.1038/nature11360>
- Palmer, M. R., & Elderfield, H. (1985). Sr isotope composition of sea water over the past 75 Myr. *Nature*, *314*(6011), 526–528. <https://doi.org/10.1038/314526a0>
- Pearce, C. R., Parkinson, I. J., Gaillardet, J., Charlier, B. L. A., Mokadem, F., & Burton, K. W. (2015). Reassessing the stable ($\delta^{88/86}\text{Sr}$) and radiogenic ($^{87}\text{Sr}/^{86}\text{Sr}$) strontium isotopic composition of marine inputs. *Geochimica et Cosmochimica Acta*, *157*, 125–146. <https://doi.org/10.1016/j.gca.2015.02.029>
- Pettke, T., Halliday, A. N., Hall, C. M., & Rea, D. K. (2000). Dust production and deposition in Asia and the North Pacific Ocean over the past 12 Myr. *Earth and Planetary Science Letters*, *178*(3–4), 397–413. [https://doi.org/10.1016/S0012-821X\(00\)00083-2](https://doi.org/10.1016/S0012-821X(00)00083-2)
- Pettke, T., Halliday, A. N., & Rea, D. K. (2002). Cenozoic evolution of Asian climate and sources of Pacific seawater Pb and Nd derived from eolian dust of sediment core LL44-GPC3. *Paleoceanography*, *17*(3), 3-1–3-13. <https://doi.org/10.1029/2001PA000673>
- Plank, T., Kelley, K. A., Murray, R. W., & Stern, L. Q. (2007). Chemical composition of sediments subducting at the Izu-Bonin trench. *Geochemistry, Geophysics, Geosystems*, *8*(4), 1. <https://doi.org/10.1029/2006GC001444>
- Plank, T., & Langmuir, C. H. (1998). The chemical composition of subducting sediment and its consequences for the crust and mantle. *Chemical Geology*, *145*(3–4), 325–394. [https://doi.org/10.1016/S0009-2541\(97\)00150-2](https://doi.org/10.1016/S0009-2541(97)00150-2)
- Pourmand, A., Dauphas, N., & Ireland, T. J. (2012). A novel extraction chromatography and MC-ICP-MS technique for rapid analysis of REE, Sc and Y: Revising CI-chondrite and Post-Archean Australian Shale (PAAS) abundances. *Chemical Geology*, *291*, 38–54. <https://doi.org/10.1016/j.chemgeo.2011.08.011>
- Ravizza, G. E., & Zachos, J. C. (2014). Records of Cenozoic Ocean Chemistry. In H. D. Holland, & K. K. Turekian (Eds.), *Treatise on Geochemistry* (Vol. 8, pp. 543–568). Elsevier. <https://doi.org/10.1016/B978-0-08-095975-7.00620-3>
- Rea, D. K. (1994). The paleoclimatic record provided by eolian deposition in the deep sea: The geologic history of wind. *Reviews of Geophysics*, *32*(2), 159–195. <https://doi.org/10.1029/93RG03257>
- Robertson, A. H. F., Kutterolf, S., Avery, A., Baxter, A. T., Petronotis, K., Acton, G. D., et al. (2018). Depositional setting, provenance, and tectonic-volcanic setting of Eocene–Recent deep-sea sediments of the oceanic Izu–Bonin forearc, northwest Pacific (IODP Expedition 352). *International Geology Review*, *60*(15), 1816–1854. <https://doi.org/10.1080/00206814.2017.1393634>
- Savov, I. P., Hickey-Vargas, R., D'Antonio, M., Ryan, J. G., & Spadea, P. (2006). Petrology and geochemistry of west philippine basin basalts and early Palau-Kyushu arc volcanic clasts from ODP Leg 195, site 1201D: Implications for the early history of the Izu-Bonin-Mariana arc. *Journal of Petrology*, *47*(2), 277–299. <https://doi.org/10.1093/petrology/egi075>
- Schindlbeck, J. C., Kutterolf, S., Straub, S. M., Andrews, G. D. M., Wang, K. L., & Mleneck-Vautravets, M. J. (2018). One million years tephra record at IODP sites U1436 and U1437: Insights into explosive volcanism from the Japan and Izu arcs. *Island Arc*, *27*(3), e12244. <https://doi.org/10.1111/iar.12244>
- Scudder, R. P., Murray, R. W., Schindlbeck, J. C., Kutterolf, S., Hauff, F., & Mckinley, C. C. (2014). Regional-scale input of dispersed and discrete volcanic ash to the Izu-Bonin and Mariana subduction zones. *Geochemistry, Geophysics, Geosystems*, *15*(11), 4369–4379. <https://doi.org/10.1002/2014GC005561>
- Shipboard Scientific Party. (1990). Site 801. In Y. Lancelot, & L. Larson (Eds.), *Proceedings of the Ocean Drilling Program, 129 initial reports* (Vol. 129, pp. 91–170). Ocean Drilling Program. <https://doi.org/10.2973/odp.proc.ir.129.103.1990>
- Shipboard Scientific Party. (2002). Site 1201. In M. H. Salisbury, M. Shinohara, C. Richter, & E. Al (Eds.), *Proceedings of the Ocean Drilling Program, 195 initial reports* (Vol. 195, pp. 1–233). Ocean Drilling Program. <https://doi.org/10.2973/odp.proc.ir.195.104.2002>
- Sigurdsson, H., Kelley, S., Leckie, R. M., Carey, S., Bralower, T., & King, J. (2000). History of circum-Caribbean explosive volcanism: $^{40}\text{Ar}/^{39}\text{Ar}$ dating of tephra layers. *Proceedings of the Ocean Drilling Program: Scientific Results*, *165*, 299–314. <https://doi.org/10.2973/odp.proc.sr.165.021.2000>
- Sinton, C. W., Duncan, R. A., Storey, M., Lewis, J., & Estrada, J. J. (1998). An oceanic flood basalt province within the Caribbean plate. *Earth and Planetary Science Letters*, *155*(3–4), 221–235. [https://doi.org/10.1016/S0012-821X\(97\)00214-8](https://doi.org/10.1016/S0012-821X(97)00214-8)
- Stancin, A. M., Gleason, J. D., Rea, D. K., Owen, R. M., Moore, T. C., Blum, J. D., & Hovan, S. A. (2006). Radiogenic isotopic mapping of late Cenozoic eolian and hemipelagic sediment distribution in the east-central Pacific. *Earth and Planetary Science Letters*, *248*, 840–850. <https://doi.org/10.1016/j.epsl.2006.06.038>
- Stonacipher, S. A. (1976). Origin, distribution and diagenesis of phillipsite and clinoptilolite in deep-sea sediments. *Chemical Geology*, *17*(1–4), 307–318. [https://doi.org/10.1016/0009-2541\(76\)90044-9](https://doi.org/10.1016/0009-2541(76)90044-9)
- Straub, S. M., Goldstein, S. L., Class, C., Schmidt, A., & Gomez-Tuena, A. (2010). Slab and mantle controls on the Sr-Nd-Pb-Hf isotope evolution of the Post 42 Ma Izu-Bonin volcanic arc. *Journal of Petrology*, *51*(5), 993–1026. <https://doi.org/10.1093/petrology/egq009>
- Straub, S. M., Woodhead, J. D., & Arculus, R. J. (2015). Temporal evolution of the Mariana Arc: Mantle wedge and subducted slab controls revealed with a tephra perspective. *Journal of Petrology*, *56*(2), 409–439. <https://doi.org/10.1093/petrology/egv005>
- Straub, S. M., Woodhead, J. D., & Arculus, R. J. (2017). *Major and trace elements and Sr-Nd-Pb-Hf of 0-43 Ma fallout tephra from the Mariana Island Arc*. <https://doi.org/10.1594/IEDA/100660>
- Sun, J. (2005). Nd and Sr isotopic variations in Chinese eolian deposits during the past 8 Ma: Implications for provenance change. *Earth and Planetary Science Letters*, *240*(2), 454–466. <https://doi.org/10.1016/j.epsl.2005.09.019>
- Sun, J., & Zhu, X. (2010). Temporal variations in Pb isotopes and trace element concentrations within Chinese eolian deposits during the past 8 Ma: Implications for provenance change. *Earth and Planetary Science Letters*, *290*(3–4), 438–447. <https://doi.org/10.1016/j.epsl.2010.01.001>
- Takahashi, T., Hirahara, Y., Miyazaki, T., Vaglarov, B. S., Chang, Q., Kimura, J., & Tatsumi, Y. (2009). *Precise determination of Sr isotope ratios in igneous rock samples and application to micro-analysis of plagioclase phenocrysts* (Vol. 2009, pp. 59–64). JAMSTEC Report of Research and Development. <https://doi.org/10.5918/jamstecr.2009.59>
- Takahashi, Y., Manceau, A., Geoffroy, N., Marcus, M. A., & Usui, A. (2007). Chemical and structural control of the partitioning of Co, Ce, and Pb in marine ferromanganese oxides. *Geochimica et Cosmochimica Acta*, *71*(4), 984–1008. <https://doi.org/10.1016/j.gca.2006.11.016>

- Takahashi, Y., Shimizu, H., Usui, A., Kagi, H., & Nomura, M. (2000). Direct observation of tetravalent cerium in ferromanganese nodules and crusts by X-ray-absorption near-edge structure (XANES). *Geochimica et Cosmochimica Acta*, *64*(17), 2929–2935. [https://doi.org/10.1016/S0016-7037\(00\)00403-8](https://doi.org/10.1016/S0016-7037(00)00403-8)
- Takaya, Y., Yasukawa, K., Kawasaki, T., Fujinaga, K., Ohta, J., Usui, Y., et al. (2018). The tremendous potential of deep-sea mud as a source of rare-earth elements. *Scientific Reports*, *8*(1), 5763. <https://doi.org/10.1038/s41598-018-23948-5>
- Tanaka, E., Nakamura, K., Yasukawa, K., Mimura, K., Fujinaga, K., Iijima, K., et al. (2020). Chemostratigraphy of deep-sea sediments in the western North Pacific Ocean: Implications for genesis of mud highly enriched in rare-earth elements and yttrium. *Ore Geology Reviews*, *119*, 103392. <https://doi.org/10.1016/j.oregeorev.2020.103392>
- Tanaka, E., Nakamura, K., Yasukawa, K., Mimura, K., Fujinaga, K., Ohta, J., et al. (2020). Chemostratigraphic correlations of Deep-sea sediments in the western North Pacific Ocean: A new constraint on the distribution of mud highly enriched in rare-earth elements. *Minerals*, *10*(6), 575. <https://doi.org/10.3390/min10060575>
- Taylor, B. (1992). Rifting and the volcanic-tectonic evolution of the Izu-Bonin-Mariana arc. In *Proceedings of the Ocean Drilling Program, 126 Scientific Results* (Vol. 126, pp. 627–652). Ocean Drilling Program. <https://doi.org/10.2973/odp.proc.sr.126.163.1992>
- Taylor, B., & Goodliffe, A. M. (2004). The West Philippine Basin and the initiation of subduction, revisited. *Geophysical Research Letters*, *31*(12), L12602. <https://doi.org/10.1029/2004GL020136>
- Taylor, S. R., McLennan, S. M., & McCulloch, M. T. (1983). Geochemistry of loess, continental crustal composition and crustal model ages. *Geochimica et Cosmochimica Acta*, *47*(11), 1897–1905. [https://doi.org/10.1016/0016-7037\(83\)90206-5](https://doi.org/10.1016/0016-7037(83)90206-5)
- Toyoda, K., Nakamura, Y., & Masuda, A. (1990). Rare earth elements of Pacific pelagic sediments. *Geochimica et Cosmochimica Acta*, *54*(4), 1093–1103. [https://doi.org/10.1016/0016-7037\(90\)90441-M](https://doi.org/10.1016/0016-7037(90)90441-M)
- Trueman, C. N., & Tuross, N. (2002). Trace elements in recent and fossil bone apatite. *Reviews in Mineralogy and Geochemistry*, *48*(1), 489–521. <https://doi.org/10.2138/rmg.2002.48.13>
- Uramoto, G. I., Morono, Y., Tomioka, N., Wakaki, S., Nakada, R., Wagai, R., et al. (2019). Significant contribution of seafloor microparticles to the global manganese budget. *Nature Communications*, *10*(1), 1–10. <https://doi.org/10.1038/s41467-019-08347-2>
- Usui, A., Nishi, K., Sato, H., Nakasato, Y., Thornton, B., Kashiwbara, T., et al. (2017). Continuous growth of hydrogenetic ferromanganese crusts since 17 Myr ago on Takuyo-Daigo Seamount, NW Pacific, at water depths of 800–5500 m. *Ore Geology Reviews*, *87*, 71–87. <https://doi.org/10.1016/j.oregeorev.2016.09.032>
- Usui, Y., & Yamazaki, T. (2021). Magnetostratigraphic evidence for post-depositional distortion of osmium isotopic records in pelagic clay and its implications for mineral flux estimates. *Earth Planets and Space*, *73*(1), 2. <https://doi.org/10.1186/s40623-020-01338-4>
- Usui, Y., Yamazaki, T., & Saitoh, M. (2017). Changing abundance of magnetofossil morphologies in pelagic red clay around Minamitorishima, western North Pacific. *Geochemistry, Geophysics, Geosystems*, *18*(12), 4558–4572. <https://doi.org/10.1002/2017GC007127>
- Van Andel, T. H. (1975). Mesozoic/Cenozoic calcite compensation depth and the global distribution of calcareous sediments. *Earth and Planetary Science Letters*, *26*, 187–194. [https://doi.org/10.1016/0012-821X\(75\)90086-2](https://doi.org/10.1016/0012-821X(75)90086-2)
- van de Fliert, T., Frank, M., Lee, D. C., Halliday, A. N., Reynolds, B. C., & Hein, J. R. (2004). New constraints on the sources and behavior of neodymium and hafnium in seawater from Pacific Ocean ferromanganese crusts. *Geochimica et Cosmochimica Acta*, *19*, 3827–3843. <https://doi.org/10.1016/j.gca.2004.03.009>
- Veizer, J., Ala, D., Azmy, K., Bruckschen, P., Buhl, D., Bruhn, F., et al. (1999). $^{87}\text{Sr}/^{86}\text{Sr}$, $\delta^{13}\text{C}$ and $\delta^{18}\text{O}$ evolution of Phanerozoic seawater. *Chemical Geology*, *161*(1–3), 59–88. [https://doi.org/10.1016/S0009-2541\(99\)00081-9](https://doi.org/10.1016/S0009-2541(99)00081-9)
- Vervoort, J. D., Plank, T., & Prytulak, J. (2011). The Hf-Nd isotopic composition of marine sediments. *Geochimica et Cosmochimica Acta*, *75*(20), 5903–5926. <https://doi.org/10.1016/j.gca.2011.07.046>
- White, W. M., & Klein, E. M. (2014). Composition of the oceanic crust. In H. D. Holland, & K. K. Turekian (Eds.), *Treatise on Geochemistry* (2nd ed., pp. 457–496). Elsevier. <https://doi.org/10.1016/B978-0-08-095975-7.00315-6>
- Yasukawa, K., Kino, S., Azami, K., Tanaka, E., Mimura, K., Ohta, J., et al. (2020). Geochemical features of Fe-Mn micronodules in deep-sea sediments of the western North Pacific Ocean: Potential for co-product metal extraction from REY-rich mud. *Ore Geology Reviews*, *127*, 103805. <https://doi.org/10.1016/j.oregeorev.2020.103805>
- Yasukawa, K., Kino, S., Ohta, J., Azami, K., Tanaka, E., Mimura, K., et al. (2021). Stratigraphic variations of Fe–Mn micronodules and implications for the formation of extremely REY-rich mud in the western North Pacific Ocean. *Minerals*, *11*(3), 1–20. <https://doi.org/10.3390/min11030270>
- Yasukawa, K., Liu, H., Fujinaga, K., Machida, S., Haraguchi, S., Ishii, T., et al. (2014). Geochemistry and mineralogy of REY-rich mud in the eastern Indian Ocean. *Journal of Asian Earth Sciences*, *93*, 25–36. <https://doi.org/10.1016/j.jseaes.2014.07.005>
- Yasukawa, K., Nakamura, K., Fujinaga, K., Iwamori, H., & Kato, Y. (2016). Tracking the spatiotemporal variations of statistically independent components involving enrichment of rare-earth elements in deep-sea sediments. *Scientific Reports*, *6*(1), 29603. <https://doi.org/10.1038/srep29603>
- Yasukawa, K., Ohta, J., Miyazaki, T., Vaglarov, B. S., Chang, Q., Ueki, K., et al. (2019). Statistic and isotopic characterization of deep-sea sediments in the western North Pacific Ocean: Implications for genesis of the sediment extremely enriched in rare earth elements. *Geochemistry, Geophysics, Geosystems*, *20*(7), 3402–3430. <https://doi.org/10.1029/2019GC008214>
- Yokoo, Y., Nakano, T., Nishikawa, M., & Quan, H. (2004). Mineralogical variation of Sr-Nd isotopic and elemental compositions in loess and desert sand from the central Loess Plateau in China as a provenance tracer of wet and dry deposition in the northwestern Pacific. *Chemical Geology*, *204*(1–2), 45–62. <https://doi.org/10.1016/j.chemgeo.2003.11.004>
- Zhang, W., Chen, J., Ji, J., & Li, G. (2016). Evolving flux of Asian dust in the north Pacific Ocean since the late Oligocene. *Aeolian Research*, *23*, 11–20. <https://doi.org/10.1016/j.aeolia.2016.09.004>
- Zhou, L., & Kyte, F. T. (1992). Sedimentation history of the South Pacific pelagic clay province over the last 85 million years Inferred from the geochemistry of Deep Sea Drilling Project Hole 596. *Paleoceanography*, *7*(4), 441–465. <https://doi.org/10.1029/92PA01063>

References From the Supporting Information

- Alibo, D. S., & Nozaki, Y. (1999). Rare earth elements in seawater: Particle association, shale-normalization, and Ce oxidation. *Geochimica et Cosmochimica Acta*, *63*(3–4), 363–372. [https://doi.org/10.1016/S0016-7037\(98\)00279-8](https://doi.org/10.1016/S0016-7037(98)00279-8)
- Aries, S., Valladon, M., Polvé, M., & Dupré, B. (2000). A routine method for oxide and hydroxide interference corrections in ICP-MS chemical analysis of environmental and geological samples. *Geostandards Newsletter*, *24*(1), 19–31. <https://doi.org/10.1111/j.1751-908X.2000.tb00583.x>

- Barrett, T. J., & Jarvis, I. (1988). Rare-earth element geochemistry of metalliferous sediments from DSDP Leg 92: The East Pacific Rise transect. *Chemical Geology*, 67(3–4), 243–259. [https://doi.org/10.1016/0009-2541\(88\)90131-3](https://doi.org/10.1016/0009-2541(88)90131-3)
- Li, G., & Elderfield, H. (2013). Evolution of carbon cycle over the past 100 million years. *Geochimica et Cosmochimica Acta*, 103, 11–25.
- Zhang, J., & Nozaki, Y. (1996). Rare earth elements and yttrium in seawater: ICP-MS determinations in the East Caroline, Coral Sea, and South Fiji basins of the western South Pacific Ocean. *Geochimica et Cosmochimica Acta*, 60(23), 4631–4644. [https://doi.org/10.1016/S0016-11327037\(96\)00276-1](https://doi.org/10.1016/S0016-11327037(96)00276-1)